Geophysical Journal International

Geophys. J. Int. (2015) **200,** 1172–1195
GJI Seismology

doi: 10.1093/gji/ggu459

Induced seismicity constraints on subsurface geological structure, Paradox Valley, Colorado

Lisa V. Block, Christopher K. Wood, William L. Yeck and Vanessa M. King

U.S. Department of the Interior, Bureau of Reclamation, P.O. Box 25007, *Code* 86-68330, *Denver, CO* 80225, *USA. E-mail:* lblock@usbr.gov

Accepted 2014 December 1. Received 2014 October 17; in original form 2014 May 8

SUMMARY

Precise relative hypocentres of seismic events induced by long-term fluid injection at the Paradox Valley Unit (PVU) brine disposal well provide constraints on the subsurface geological structure and compliment information available from deep seismic reflection and well data. We use the 3-D spatial distribution of the hypocentres to refine the locations, strikes, and throws of subsurface faults interpreted previously from geophysical surveys and to infer the existence of previously unidentified subsurface faults. From distinct epicentre lineations and focal mechanism trends, we identify a set of conjugate fracture orientations consistent with shear-slip reactivation of late-Palaeozoic fractures over a widespread area, as well as an additional fracture orientation present only near the injection well. We propose simple Mohr–Coulomb fracture models to explain these observations. The observation that induced seismicity preferentially occurs along one of the identified conjugate fracture orientations can be explained by a rotation in the direction of the regional maximum compressive stress from the time when the fractures were formed to the present. Shear slip along the third fracture orientation observed near the injection well is inconsistent with the current regional stress field and suggests a local rotation of the horizontal stresses. The detailed subsurface model produced by this analysis provides important insights for anticipating spatial patterns of future induced seismicity and for evaluation of possible additional injection well sites that are likely to be seismically and hydrologically isolated from the current well. In addition, the interpreted fault patterns provide constraints for estimating the maximum magnitude earthquake that may be induced, and for building geomechanical models to simulate pore pressure diffusion, stress changes and earthquake triggering.

Key words: Geomechanics; Fracture and flow; Earthquake dynamics; Dynamics and mechanics of faulting; Dynamics: seismotectonics; Fractures and faults.

INTRODUCTION

Knowledge of the subsurface geological structure in the vicinity of an injection well used for fluid disposal is essential for modelling the long-term behaviour and evolution of the subsurface reservoir. Key elements in developing this knowledge include identification of permeable zones for fluid transport and storage, confirmation of the presence of an adequate confining layer, estimation of formation storage capacity and identification of faults that may act as impermeable boundaries or potentially serve as sources of induced seismicity. Modern geophysical techniques, such as deep seismic reflection surveys and geophysical well logging, are widely used for interpreting subsurface geological structure. However, the application of these methods can be limited by land access issues, poor data quality, and expense. In addition, faults with dominant strike-slip motion, having negligible vertical offset, can be difficult to resolve on seismic reflection data.

While the use of microseismic monitoring to understand reservoir characteristics and behaviour is not new, recent developments have increased the ability of researchers to recognize individual faults and fractures. For example, waveform cross-correlation techniques increase the accuracy of relative hypocentre locations and allow seismicity to be clustered by type, both in the time domain (e.g. Rowe *et al.* 2002; Snieder & Vrijlandt 2005; Song *et al.* 2010) and in the frequency domain (Fagan *et al.* 2013). Shear wave splitting observed within induced seismicity data has also been analysed to determine variations in stress directions, characterize fracture sets and study the temporal evolution of fractures (Winterstein & Meadows 1991; Sayers 1998; Wuestefeld *et al.* 2011).

We demonstrate that precise relative hypocentres of earthquakes induced by long-term fluid disposal at the Paradox Valley Unit (PVU) injection well provide supplemental constraints on the subsurface geological structure over distances of several kilometres (km) from the well. Specifically, we use the spatial and temporal patterns of recorded microseismicity to revise the previous subsurface fault model and propose two alternative new models. We use these revised models to delineate the area that has likely experienced substantial pore pressure increase from current injection operations

Published by Oxford University Press on behalf of The Royal Astronomical Society 2015. This work is written by (a) US Government employee(s) and is in the public domain in the US.

Downloaded from http://gji.oxfordjournals.org/ by guest on January 7, 2015

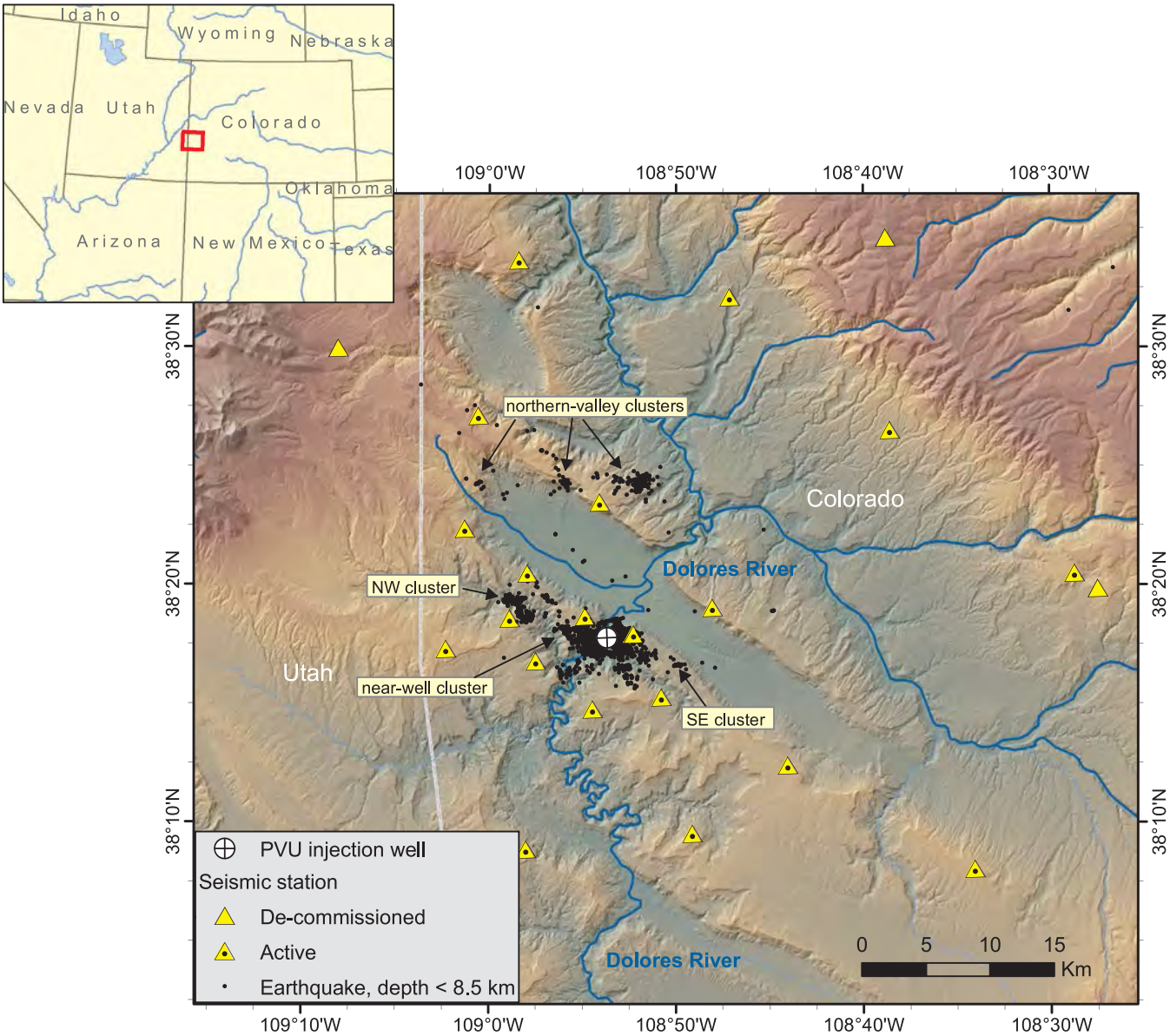

Figure 1. Location of the Paradox Valley Unit (PVU) injection well and the Paradox Valley Seismic Network (PVSN) stations. The labelled earthquake clusters are discussed in the text.

and to identify pre-existing faults that are preferentially oriented for shear failure. One of the new models also indicates an area that may be only marginally affected by current injection operations and may therefore warrant further investigation for site selection of a potential second injection well.

BACKGROUND

The PVU

The PVU disposes of naturally occurring brine in a single injection well in western Colorado (Fig. 1). The project is a component of the Colorado River Basin Salinity Control Program, an effort to improve water quality in the Colorado River system. PVU intercepts highly saline groundwater flows that would otherwise enter the Dolores River, a tributary of the Colorado River, and injects the brine into a 4.8-km-deep well. PVU has been injecting brine almost continuously since mid-1996. A series of injection tests conducted between 1991 and 1995 preceded long-term injection. Calculated downhole injection pressures at the depth of the target formation are often above the estimated fracture propagation pressure of approximately 70 MPa and have reached values as high as 84 MPa. Daily average flow rates have been variable, generally ranging from $\sim 1.5 \times 10^{-2}$ to $\sim 2.2 \times 10^{-2}$ m^3 s^{-1} ($\sim$230–345 Gal min^{-1}) during long-term injection (Fig. 2). To date, 7.7 million cubic metres of fluid have been injected.

Seismic monitoring has been an integral part of PVU throughout the history of the project. The Paradox Valley Seismic Network (PVSN), a surface array originally consisting of ten vertical-component seismic stations, was installed to determine the pre-injection baseline level of local seismicity and to subsequently record seismic events induced by PVU fluid injection. PVSN has been continuously operational since 1985, 6 yr prior to the first

Downloaded from http://gji.oxfordjournals.org/ by guest on January 7, 2015

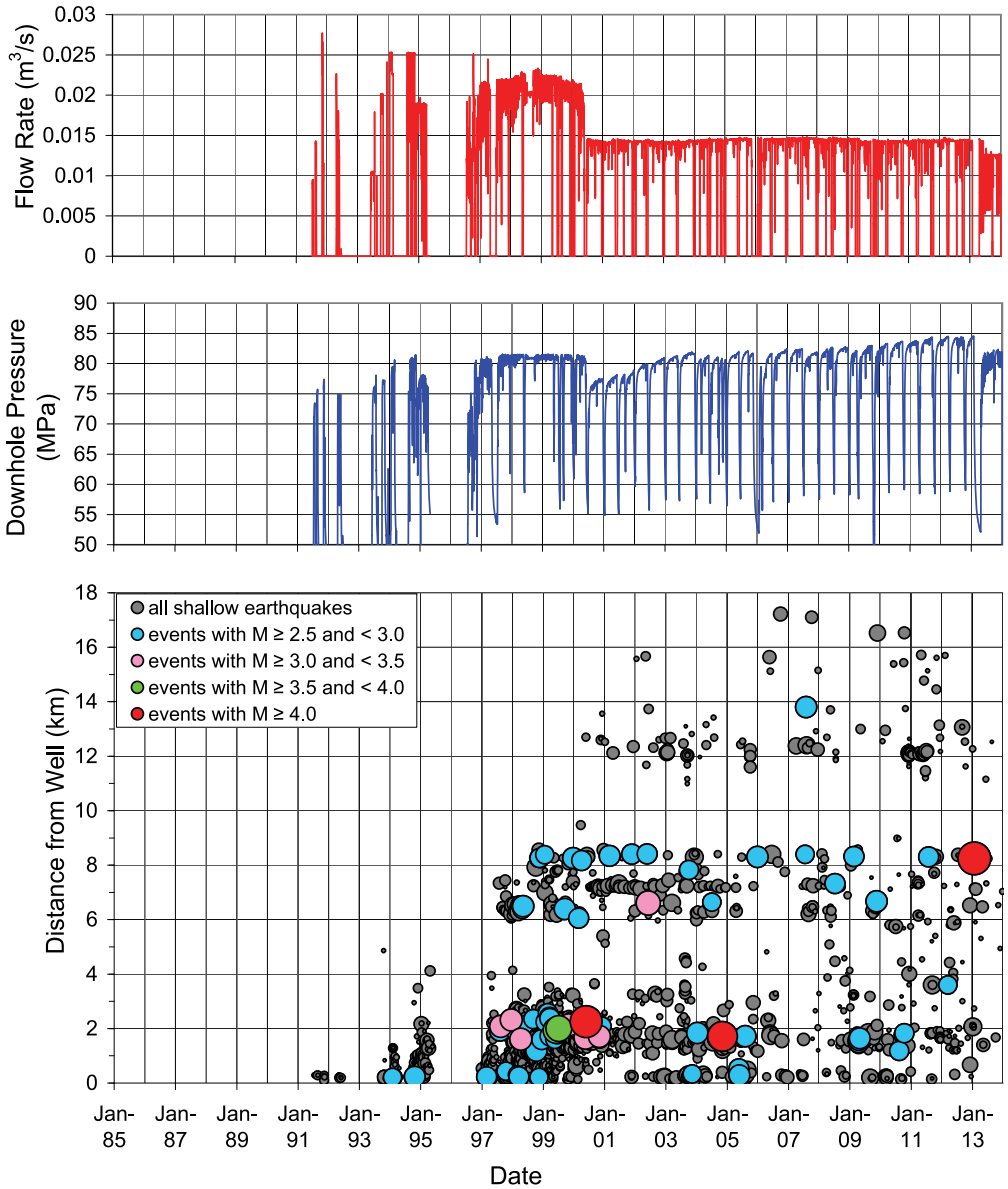

Figure 2. Scatter plot of earthquakes having $M \geq 0.5$ and depth <8.5 km (relative to the ground surface elevation at the PVU injection wellhead), plotted as a function of date and distance from the PVU injection well (lower plot). Each circle represents a single earthquake, with the width of the circle scaled by the event magnitude. The upper plots show the daily average injection flow rate into the PVU well and the calculated downhole pressure at the depth of the primary target injection formation (4.3 km).

PVU injection test. Over time, PVSN has been expanded and updated, and the network currently consists of 20 three-component broadband digital surface seismometers (Fig. 1).

The U.S. Department of the Interior, Bureau of Reclamation (Reclamation), operates the PVU brine extraction, injection, and seismic monitoring programs. The PVU well is permitted by the Environment Protection Agency (EPA) as a Class V injection well, and the seismic monitoring program is a requirement of the injection permit. Reclamation analyses the recorded seismic data on a continual basis and reports all seismic activity to EPA annually.

Local geology

Paradox Valley is located in the Paradox fold and fault belt and was formed by the collapse of a northwest-trending diapiric salt-cored anticline (Cater 1970; Gutierrez 2004; Trudgill 2011). The PVU injection well is located on the southwest flank of the salt anticline (Fig. 3). The well penetrates Triassic- through Cambrian-age sedimentary rock layers and granitic Precambrian basement. With the exception of the Paradox formation, which consists primarily of highly deformed salt layers, the geological units are generally subhorizontal. The basement and overlying sedimentary layers are offset by a series of northwest-striking high-angle normal faults, which result in an overall deepening of the rock units toward the northeast (Fig. 3). These deep faults do not extend to the ground surface. Their locations have been mapped using deep seismic reflection and well log data but are only approximately known (Block *et al.* 2012; King *et al.* 2014).

Based on interpretation of regional core and log data, Reclamation selected the Mississippian Leadville carbonate as the primary injection formation. This unit has a thickness of 127 m at the PVU

Downloaded from http://gji.oxfordjournals.org/ by guest on January 7, 2015

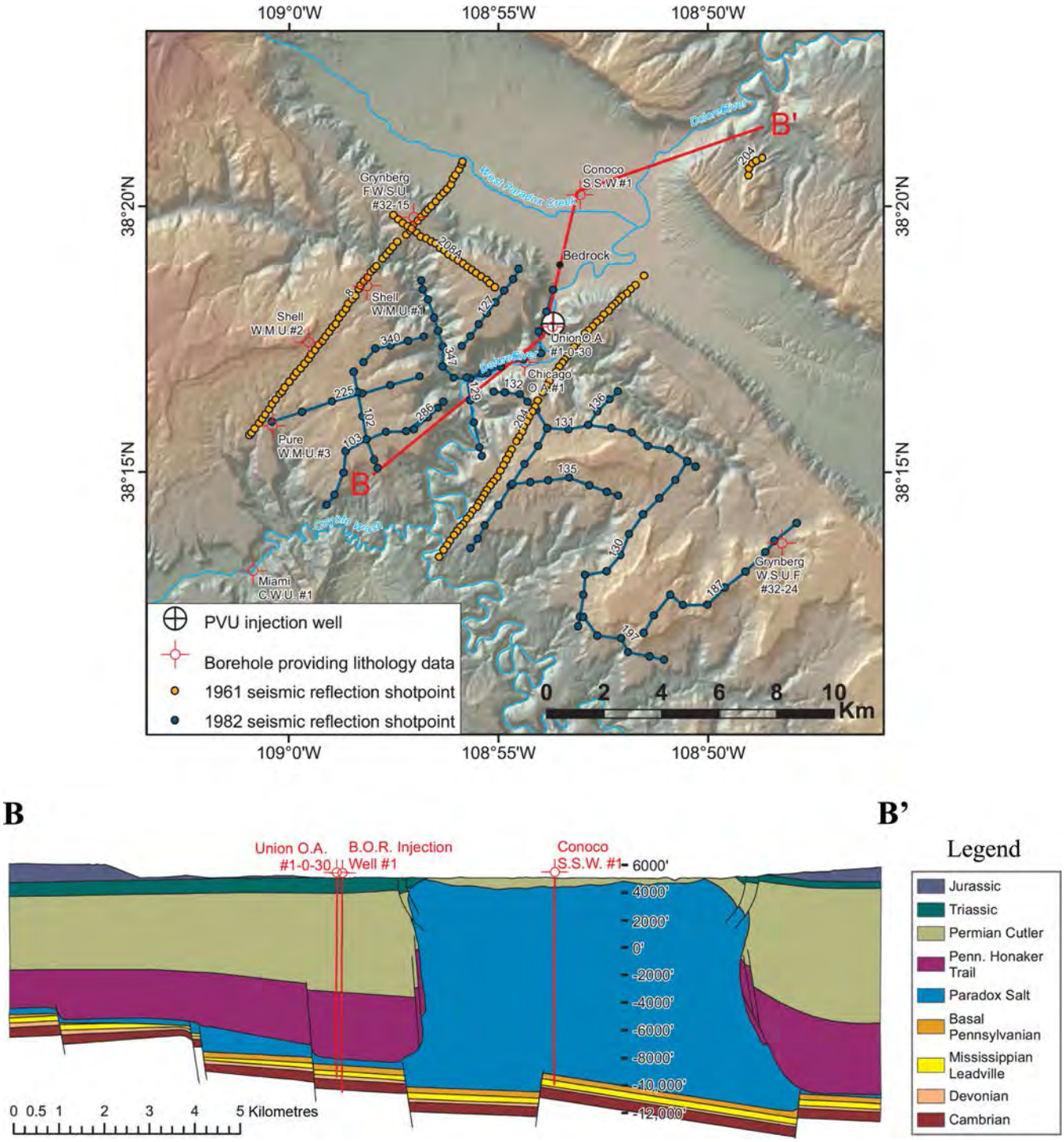

Figure 3. Location of seismic reflection lines and boreholes used to construct subsurface geological models in the vicinity of the PVU well in the mid-1980s (top panel), and geological cross section perpendicular to Paradox Valley (bottom panel). The cross section is adapted from Bremkamp & Harr (1988).

injection well site (Harr 1988). The Leadville Formation is characterized by relatively low porosity (<10 per cent) and low, fracture-dominated permeability (<10 mD; Bremkamp & Harr 1988; Envirocorp Services and Technology Inc. 1995). Geophysical logs acquired in the PVU injection well indicate 9 m of 5 per cent or greater porosity in the upper Precambrian basement, and this formation is considered a secondary target injection horizon (Bremkamp & Harr 1988). Some of the intervening early- to mid-Palaeozoic limestone and sandstone units are considered supplemental reservoirs with limited capacity. The well casing was perforated in several intervals between the top of the Leadville formation (4.3 km depth) and the bottom of the borehole (4.8 km depth). The overlying Paradox salt formation acts as a confining layer.

Prior to selecting the site for the PVU injection well, Reclamation commissioned two independent geophysical studies to analyse existing seismic reflection and well data from the area (Bremkamp *et al.* 1984; Katz & Carroll 1984). These investigations utilized 15 single-fold seismic reflection lines recorded in 1961 and reprocessed

Downloaded from http://gji.oxfordjournals.org/ by guest on January 7, 2015

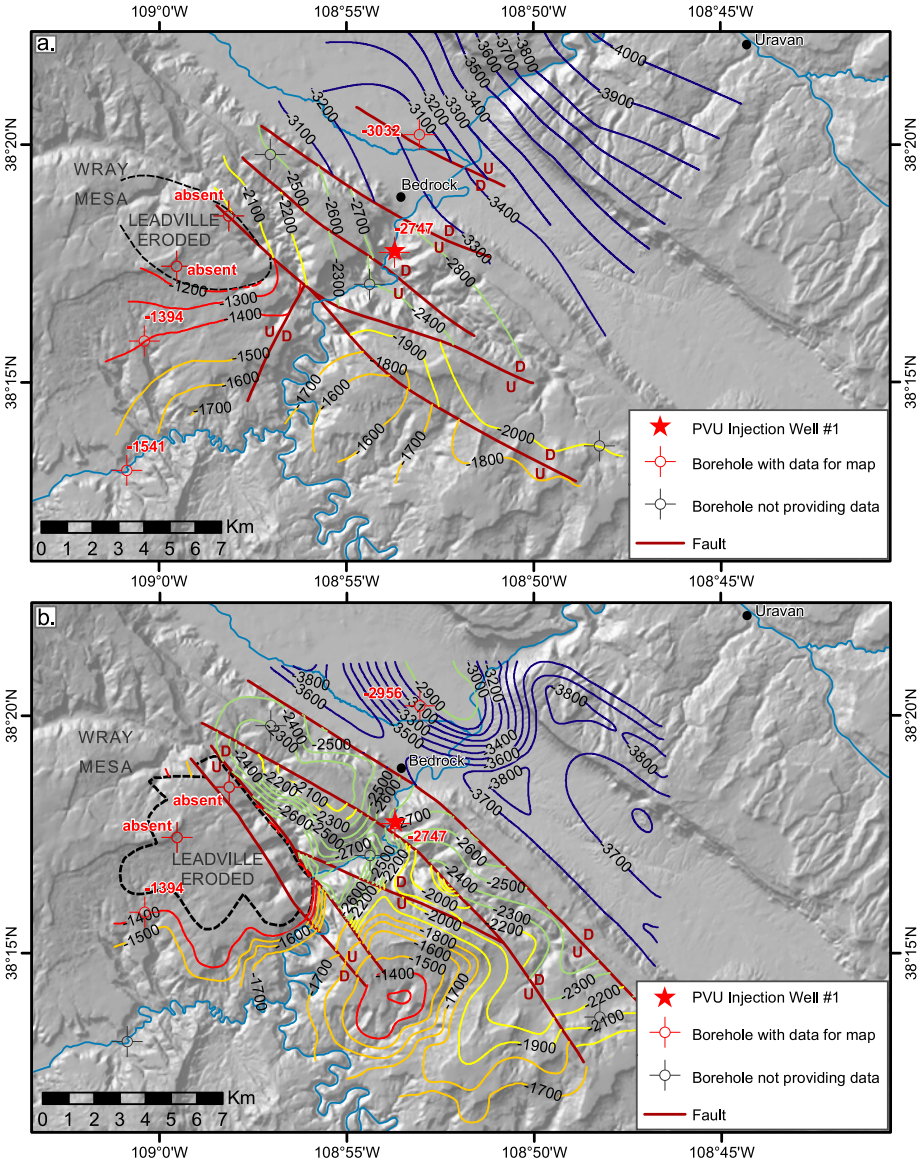

Figure 4. Structural contour maps of the top of the Leadville formation. Contour values are elevations in metres relative to mean sea level. 'U' and 'D' labels indicate the upthrown and downthrown sides of the faults, respectively. Two interpretations are shown, from Bremkamp *et al.* (1984) (top panel), and Katz & Carroll (1984) (bottom panel). Contours from both interpretations were originally drawn in feet, and were digitized, interpolated, and re-contoured with a contour interval of 50 m. Red labels indicate the elevation of the Leadville formation in the corresponding borehole.

in 1984 (blue shotpoints in Fig. 3). Additionally, Reclamation acquired three 12-fold seismic lines recorded in 1982 (gold shotpoints in Fig. 3). For both data vintages, the reports indicate that the data quality decreases greatly over thick salt sections or in areas overlain by unconsolidated material, such as in valley bottoms. The studies also used geophysical and geological logs from nine local wells as control points for formation depth and velocity (Fig. 3). Only six of the wells, however, penetrated deep enough to either reach the PVU injection target formation, the Leadville, or indicate the absence of the Leadville formation due to erosion. Each group produced top-of-formation contour maps for three geological formations, including the Leadville Formation. The maps include the interpreted locations and throws across several normal faults, which generally trend northwest-southeast (Fig. 4).

While gross features of the two independent interpretations of the same seismic reflection and well data are similar, there are also substantial differences, as illustrated by the top-of-Leadville contour maps presented in Fig. 4. Differences in the interpreted depths to the Leadville formation in the near vicinity of the injection well are as large as 300 m, nearly 2.5 times the 127-m thickness of the formation. The contour maps also indicate significant differences in the interpreted dip of the Leadville formation and in the locations, strikes, and throws of interpreted faults. A more detailed description of the two sets of interpretations is given in King *et al.* (2014).

Induced seismicity

PVSN has recorded nearly 6000 shallow earthquakes in the vicinity of Paradox Valley since injection tests began in 1991. In contrast, a comprehensive review and re-analysis of the historical PVSN database (completed in 2010) indicates only one local earthquake in the same area for the 6-yr pre-injection seismic monitoring period (1985–June 1991), and it occurred about 19 km from the PVU injection well. The vast majority of earthquakes recorded since the

Downloaded from http://gji.oxfordjournals.org/ by guest on January 7, 2015

start of injection have focal depths between 2.5 and 6.5 km depth below the injection wellhead elevation. These depths are broadly consistent with the depth range of injection (4.3–4.8 km), and the events are substantially shallower than the few naturally occurring tectonic earthquakes that have been recorded in the area during the last 30 yr, which have estimated focal depths exceeding 10 km. While most earthquakes observed since the start of injection have occurred within 4 km of the injection well, shallow seismicity has also occurred as far as 17 km from the well (Fig. 2).

The shallow seismicity recorded by PVSN has occurred at increasing distance from the PVU injection well since injection began in 1991 (Fig. 2). Within four days after the start of the first injection test in July 1991, earthquakes were detected in the immediate vicinity of the injection well. As injection continued, earthquakes were detected at progressively increasing radial distances, and, by 2002, shallow earthquakes were occurring nearly 16 km from the well (Fig. 2). Based on the almost complete lack of seismicity during 6 yr of pre-injection seismic monitoring, the general correlation of the depths of the earthquakes and the depth of injection, and the spatiotemporal evolution of the seismicity since the start of injection demonstrated in Fig. 2, we interpret the majority of the shallow earthquakes recorded since 1991 as being induced by PVU fluid injection.

Several distinct groups, or clusters, of induced seismicity have developed over the history of PVU injection (Fig. 1). By the end of the injection tests in 1995, earthquakes were occurring up to 3–4 km from the well. We refer to this area of induced seismicity immediately surrounding the injection well as the near-well region. In 1997, about 1 yr after the start of long-term injection, earthquakes began occurring 6–8 km northwest of the injection well. We identify this group of induced seismicity as the northwest (NW) cluster. In mid-2000, PVSN first detected earthquakes 12–14 km from the injection well, along the northern edge of Paradox Valley. Several distinct clusters of earthquakes have occurred along the northern edges of the valley since 2000. We refer to the earthquakes in all of these groups as northern-valley events. An earthquake was first detected about 6 km southeast of the injection well in 2004, and the seismicity rate in this area markedly increased beginning in 2010, leading to the development of a distinct earthquake cluster. We identify this compact group of earthquakes as the southeast (SE) cluster. In recent years, a few isolated earthquakes have been detected in previously aseismic areas, including beneath central Paradox Valley.

In this paper, we focus on the earthquakes recorded in the near-well area, the NW cluster, and the SE cluster, all of which are within about 9 km of the well. This region has the highest density of earthquakes, containing ∼87 per cent of all shallow (≤8.5 km depth) events recorded. The subsurface geological models derived from the seismic reflection and well data also cover much of this region. Very little seismic reflection or well data are available to provide constraints on the subsurface geological structure in seismically active areas at greater distances from the well. Finally, because the network station geometry was originally designed for detecting and accurately locating earthquakes occurring near the injection well, the computed hypocentres are more accurate for events in this region than for those occurring farther from the well.

Earthquake location methods

We calculate two sets of hypocentres from the PVSN data. Initially, we compute absolute earthquake locations using manually determined *P*- and *S*-wave arrival times. These hypocentres are computed using 3-D *P*- and *S*-wave velocity models developed from hypocentre-velocity-station correction inversions of data from naturally occurring and induced local earthquakes and explosions recorded by PVSN. Both the hypocentre-velocity inversion and earthquake location software we use were developed in-house and represent an extension of the work of Block (1991). We subsequently compute precise relative event locations from inversion of arrival time differences obtained from cross-correlations of *P*- and *S*-wave arrivals extracted from waveforms recorded at the same station for pairs of events. No time differences from manual time picks are included, with the exception of data from the five events with magnitude of 3.5 or greater. Because most of the waveforms for these events are clipped but many of the first breaks are clear, we incorporate them into the event relative location using differences of high-quality manually picked arrival times. For the relative location inversion, we use a double-difference-type algorithm. The 3-D velocity models described above are used and remain fixed during the relative location inversion. No event clustering is performed, so an event may tie to any other event in the data set. Data from event pairs with small separation distances are weighted most strongly in the inversion; data from event pairs with larger separation distances (as a fraction of the event-to-station distance) are down-weighted or eliminated from the inversion to reduce potential bias from unmodelled velocity variations in the source regions. Because the absolute earthquake locations are not well-constrained by the time difference data alone, we keep the locations of a few widely spaced (>∼3 km apart) events with well-constrained absolute locations fixed during the relative location inversion. An earthquake must tie, either directly or indirectly (possibly through multiple event pairs), to an event with a fixed location to be retained in the relative location inversion. Approximately 87 per cent of all induced earthquakes and 93 per cent of induced earthquakes with duration magnitude (M_D) ≥ 0 occurring within 10 km of the PVU injection well are considered well constrained in the relative location inversion. We assign these hypocentres a quality factor of 'a'. For the remaining events, we retain the absolute locations and assign a hypocentre quality factor of 'b'.

Both the absolute and relative location uncertainties affect the reliability of the seismicity patterns produced. When considering the relative locations of widely spaced earthquakes, the absolute location uncertainties of the events fixed during the hypocentre relative location are the most important factor. The standard errors of the absolute locations of these fixed events vary from 50 to 100 m horizontally and 70–150 m vertically. When considering the spatial distribution of closely spaced events (<∼3 km apart), the relative location uncertainties control the spatial resolution of the hypocentre patterns. Preliminary analysis of the relative location errors indicates that the error of an individual earthquake with respect to all other tied events is generally less than 50 m horizontally and 100 m vertically. Relative location errors of earthquakes in close proximity to each other are likely less, but a detailed analysis of the relative location errors as a function of event separation distance is still in progress. The absolute location errors of the events that do not tie into the relative location procedure (the b-quality events) are significantly higher, with average standard errors of approximately 500 m horizontally and 800 m vertically.

The relative hypocentres exhibit much more distinct spatial lineations than the absolute hypocentres, in both plan and cross-sectional view (Fig. 5). Because of the greater precision of the relative hypocentres compared to the absolute hypocentres, we use only the relative (a-quality) hypocentres for the geological interpretations described below.

Downloaded from http://gji.oxfordjournals.org/ by guest on January 7, 2015

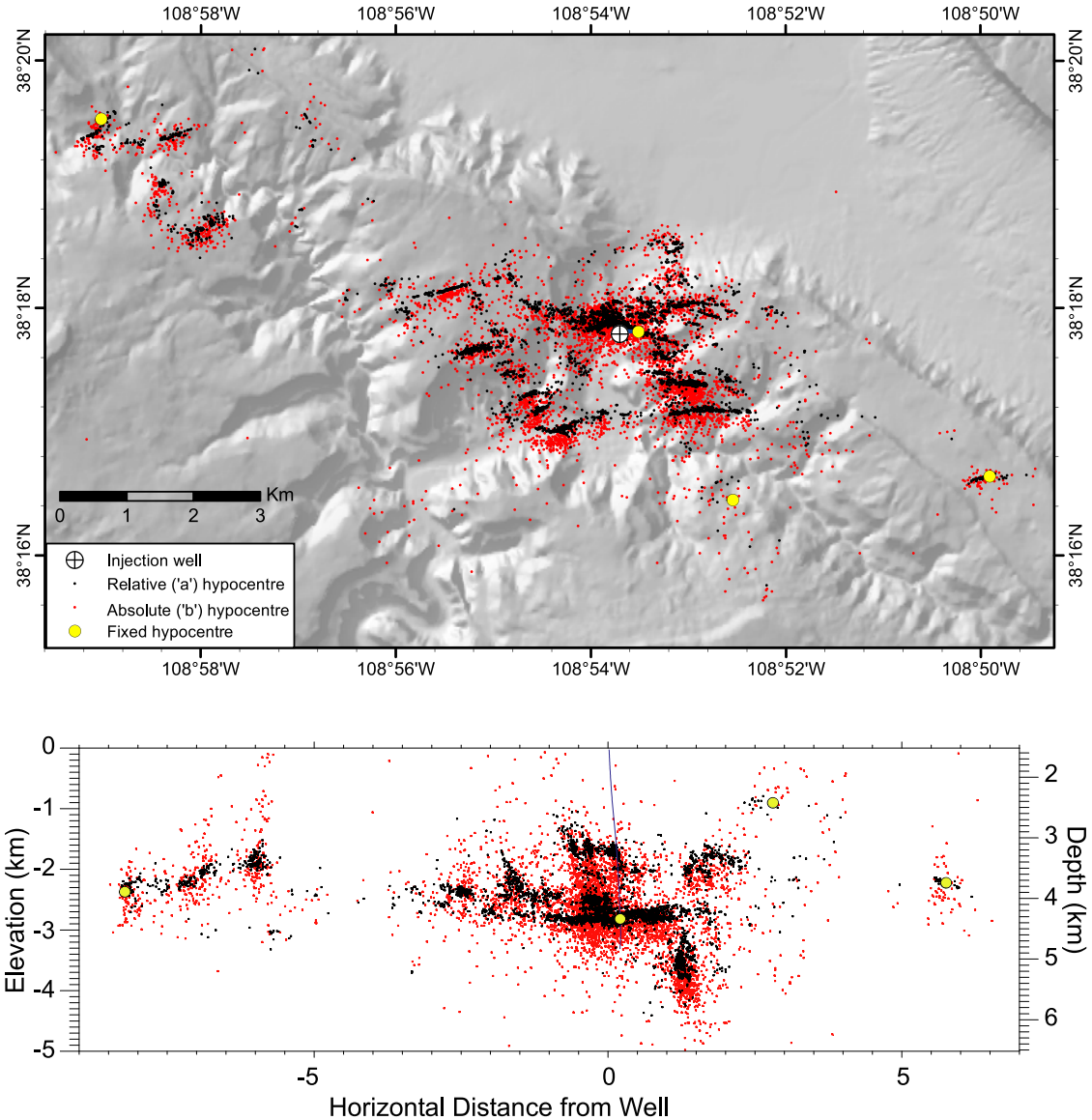

Figure 5. Absolute (red) and relative (black) hypocentres of induced earthquakes occurring southwest of Paradox Valley. The upper plot shows the hypocentres in map view, and the lower plot shows the same hypocentres projected onto a cross section parallel to Paradox Valley, looking toward the southwest. The four yellow hypocentres were fixed during the relative location inversion. Location errors of the fixed hypocentres (yellow) and relative hypocentres (black) are too small to show at this scale (<∼50–100 m).

GEOLOGICAL INTERPRETATION OF HYPOCENTRES

We propose a modification of the subsurface geological model developed in the 1980s for the region surrounding the PVU injection well, based on the spatiotemporal pattern of precise relative hypocentres of induced earthquakes. We perform our analyses from two perspectives. First, we analyse the relative elevations of clusters of hypocentres and use abrupt lateral changes in their relative elevations as an indicator of the locations of major fault blocks, assuming that hypocentres occur preferentially within the subhorizontal target injection formations. Based on the pattern of relative hypocentre elevations, we revise the locations and offsets of the northwest-striking normal faults originally identified from the seismic reflection data and propose two new alternative fault models. Second, we examine the spatial distribution and temporal evolution of distinct, linear patterns of earthquake epicentres. This leads to identification of two orientations of large-scale near-vertical fractures which we interpret as conjugate fracture sets. A third orientation of epicentre lineations near the injection well is also observed.

Our interpretations of the locations of major fault blocks depend on the assumption that the majority of the seismicity occurs within or near the target injection formations. Although the target injection formations have low to moderate permeability (<10 mD), they are significantly more permeable than other formations above or below the injection well perforations, and therefore should accept the majority of the injected and displaced *in situ* fluid. In most areas, the induced seismicity occurs in distinct clusters whose vertical extent approximately coincides with the thickness of the formations between the base of the salt confining layer and the top of the Precambrian basement (∼500 m), lending support to our assumption that most of the seismicity is occurring within or near the target formations. In some locations, scattered seismicity occurs shallower or deeper than the main seismicity clusters. These

Downloaded from http://gji.oxfordjournals.org/ by guest on January 7, 2015

events may be induced by stress changes in formations above or below the target injection interval and therefore are not considered for the construction of our geological models.

Hypocentre elevations

Based on distinct vertical offsets of nearby earthquake clusters and lateral variations in hypocentre elevation distribution in the near-well area of induced seismicity, we infer the locations of two northwest-striking normal faults west of the injection well (Faults 1 and 2, Fig. 6). Three fault blocks are created by these two normal faults (Blocks 1, 2 and 3, Fig. 6).

The location of Fault 2 is inferred by an approximate 400-m vertical offset in median hypocentre elevation. The elevations of most of the hypocentres in the immediate vicinity of the injection well, and to a distance of about 1.5 km east–northeast of the well, have elevations between −3050 and −2650 m (light and dark blue hypocentres, Fig. 6). These elevations are consistent with the known vertical extent of the Leadville formation and other subsalt Palaeozoic units encountered in the PVU injection well. However, roughly 1 km west of the injection well, at location W on the map in Fig. 6, the number of hypocentres at these elevations abruptly decreases. Southwest of location W, hypocentre depths are generally shallower, with most events occurring at elevations between −2450 and −2050 m (orange and red hypocentres). The approximate difference in median hypocentre elevation at point W is 400 m, and we interpret a northwest-striking normal fault here, down-faulted to the northeast and having a throw of roughly 400 m (Fault 2). A 400-m throw would juxtapose the Leadville formation (in Block 3, to the east) and the lower Cambrian-upper Precambrian (in Block 2, to the west), as illustrated in cross section w–w' (Fig. 6, top panel). We interpret the shallow (orange and red) hypocentres west of point W to be occurring in the primary target injection formation, the Leadville, and the relatively few deeper (blue) hypocentres west of point W to be occurring in the secondary target formations in the lower Palaeozoic and Precambrian.

We interpret the presence of another northwest-striking normal fault, also downthrown to the northeast, at location X on the map in Fig. 6 (Fault 1). At this location, nearby hypocentre clusters exhibit a distinct vertical offset of about 500 m. The hypocentres southwest of this inferred fault occur at elevations above −2050 m (grey and black hypocentres). Since the Leadville formation is the most permeable unit and therefore the formation most likely to accept injected or displaced in-situ fluid, these shallow earthquakes most likely occur within the Leadville. If this is the case, then the throw across the fault is approximately 500 m, as illustrated in cross-section x–x' (Fig. 6, bottom left-hand panel). If the shallow hypocentres are occurring within the deeper secondary target injection formations, then the throw across the fault could be greater, perhaps up to 900 m.

Approximately 1.5 km southeast of the injection well, at location Y on the map in Fig. 6, the hypocentre elevations exhibit a slightly more complex pattern than at locations W and X. Here, the occurrence of earthquakes with elevations corresponding to the Palaeozoic units in the injection well (blue hypocentres) abruptly diminishes, and we observe both a group of anomalously deep earthquakes (purple hypocentres, having elevations below −3050 m) and a group of anomalously shallow earthquakes (grey and black hypocentres, having elevations above −2050 m), as seen in cross-section y–y' (Fig. 6, bottom right-hand panel). We interpret the location of Fault 2 to be defined by the abrupt change in density of blue-coloured hypocentres. The anomalously deep earthquakes occur at this location also, suggesting that fluid may be forced down along the Fault 2 plane or through another fracture or high-permeability zone in the Precambrian. We propose that the shallow group of earthquakes (grey and black hypocentres at location Y) occur in Block 1.

The near juxtaposition of Blocks 1 and 3 at location Y may be explained by either a lateral offset of Faults 1 and 2 by a northeast-trending strike-slip fault (Fig. 7, model 1) or a merging of normal Faults 1 and 2 into a single normal fault southeast of the injection well (Fig. 7, model 2). The maps in Fig. 7 show earthquake epicentres in the near-well area and the NW and SE clusters. The hypocentres of NW-cluster earthquakes show three distinct elevation ranges, consistent with an extension of Faults 1 and 2 to the northwest. The hypocentre elevations of earthquakes occurring in the SE cluster range from about −2100 to −2300 m, consistent with those of events occurring in Block 2 in the near-well area and NW cluster (Fig. 7, orange and red hypocentres). In model 1, the SE cluster of induced seismicity is interpreted to occur in Block 2, which has been displaced to the east by about 1.5 km by the inferred strike-slip fault. In this model, the SE-cluster events are interpreted to occur mostly within the Leadville formation, as shown in the corresponding cross section z–z' (Fig. 7a). In model 2, the SE cluster of seismicity is interpreted to occur within Block 1. Assuming simple layered geology, the SE-cluster events in this model are interpreted to occur within the upper Precambrian, and no seismicity within the Leadville or other Palaeozoic formations is observed (cross-section z–z', Fig. 7b). The apparent lack of seismicity within the primary injection target formation at this location could be due to weathering and erosion of the Leadville west of Fault 1 (see discussion below). Alternatively, the SE-cluster events could be occurring within the Leadville formation if the bedding is dipping or structurally offset by one or more additional faults.

In both fault models shown in Fig. 7 we include an additional normal fault northeast of the injection well (Fault 3). The inferred existence and location of this fault is based on the interpretations from the seismic reflection data (Fig. 4) and the geographical extent of epicentres in Block 3 east of the injection well. Bremkamp *et al.* (1984) interpreted the presence of a northwest-striking normal fault very close to this location, with sufficient vertical offset to act as an impermeable boundary to fluid flow through the Leadville formation. The lack of induced seismicity east of Fault 3 supports this interpretation.

The scarcity of induced seismicity more than about 600 m southwest of Fault 1 suggests the presence of an impermeable barrier to the southwest. The geological log of the Wray Mesa Unit #1 exploration well, drilled in 1961 to a depth of 3434 m, indicates the absence of the Leadville formation (King *et al.* 2014). This well is in Block 1, at the southwest edge of the NW cluster of induced seismicity (Fig. 7). The Mississippian Leadville and underlying Devonian formations underwent extensive weathering and erosion on structural highs during late Mississippian to early Pennsylvanian time (Campbell 1981; Bremkamp & Harr 1988). In addition to thinning or removal of the Leadville, the weathered interval has significantly decreased reservoir potential due to infilling of previously porous zones with clay. If weathering and erosion occurred along a structural high parallel to Fault 1, then the absence or degradation of the primary target injection formation may inhibit fluid flow toward the southwest and explain the scarcity of induced seismicity in this region (Fig. 7). Alternatively, there could be another northwest-trending normal fault in this location with sufficient vertical offset to inhibit lateral fluid flow through the target injection formations.

Downloaded from http://gji.oxfordjournals.org/ by guest on January 7, 2015

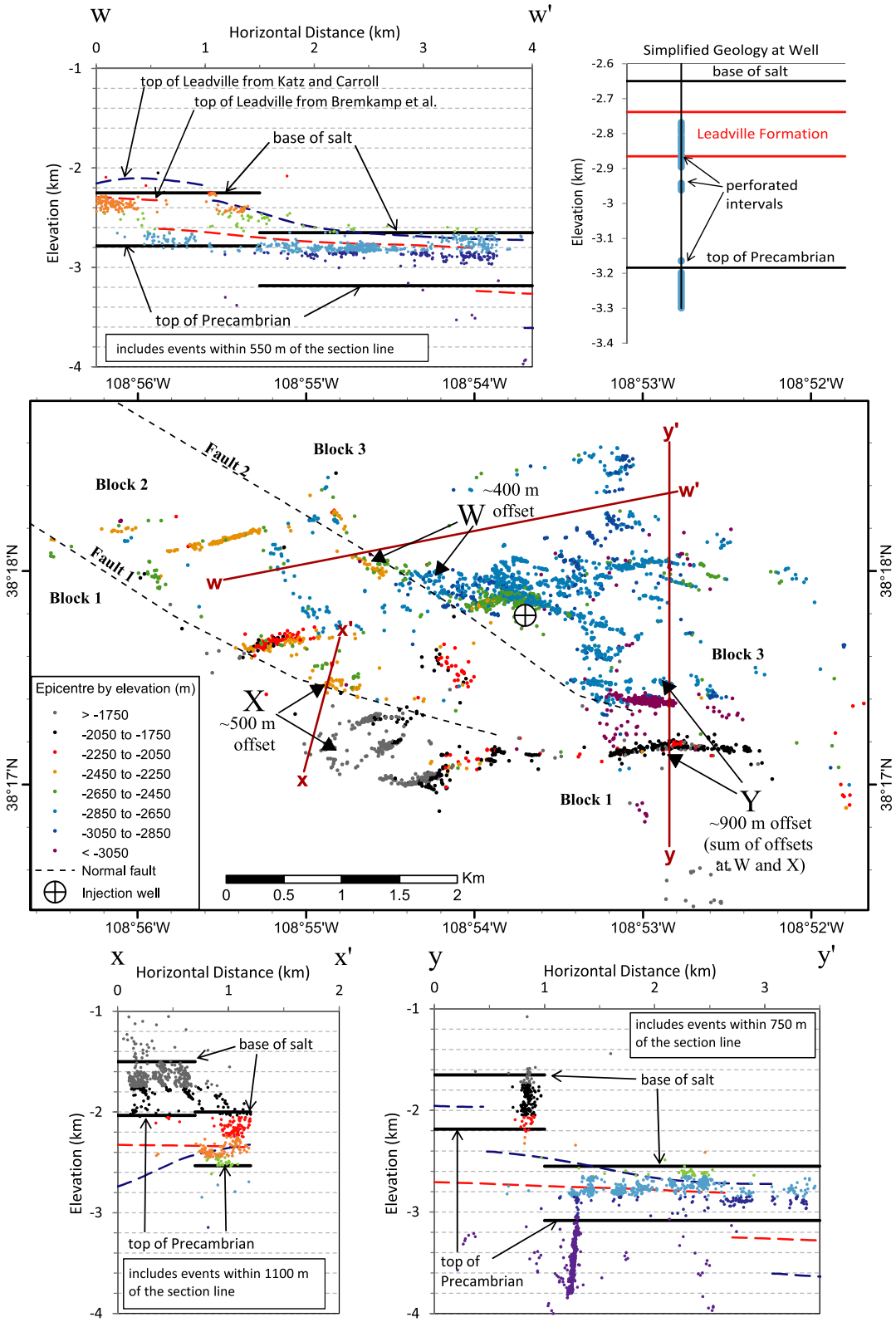

Figure 6. Map showing epicentres of earthquakes occurring in the near-well region of induced seismicity, colour-coded by hypocentre elevation (centre), and cross sections showing distinct vertical offsets of hypocentres (top and bottom). Only a-quality hypocentres from the event relative location are included. The labels 'W', 'X' and 'Y' on the map identify abrupt lateral changes in hypocentre elevations. Two northwest-striking normal faults interpreted from the hypocentre elevation patterns are shown. Our interpreted base of the Paradox salt and top of the Precambrian (solid black lines) and the interpreted top of the Leadville formation from Katz & Carroll (1984) (dashed purple line) and Bremkamp *et al.* (1984) (dashed red line) are shown in each cross section. A simplified geological section at the PVU wellbore is included at upper right for reference.

Downloaded from http://gji.oxfordjournals.org/ by guest on January 7, 2015

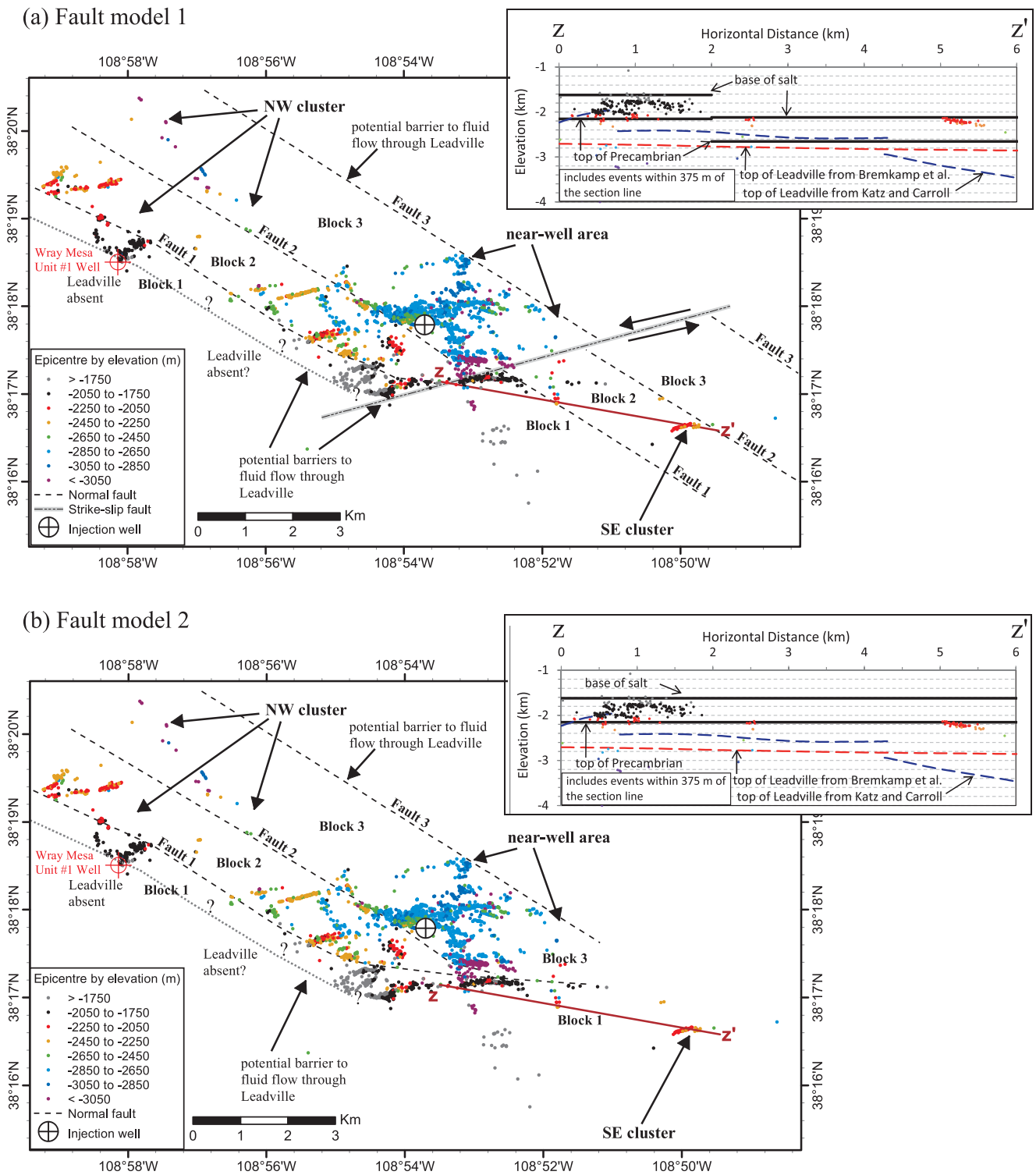

Figure 7. Maps showing epicentres of earthquakes occurring in the near-well, NW and SE clusters, colour-coded by hypocentre elevation, with interpreted faults: (a) fault model 1 (b) fault model 2. The inset cross sections show simplified interpreted geological structure between the near-well area and the SE cluster in each model. Only a-quality hypocentres from the event relative location are included. The normal faults and the fault blocks delineated by them are labelled for purposes of discussion (see text). The primary injection target formation, the Leadville, is absent in the Wray Mesa Unit #1 well shown.

Differences between the approximate elevations of the target injection formations inferred from hypocentre patterns and those interpreted from the seismic reflection data are highly variable. Close to the injection well, such as near the middle of cross-sections *w*–*w*′ and *y*–*y*′ (Fig. 6), our interpreted elevation range of target injection formations is consistent with top-of-Leadville interpretations from Katz & Carroll (1984) and Bremkamp *et al.* (1984). Farther from the injection well, however, differences between all models become much larger, as seen in cross-sections *x*–*x*′, *y*–*y*′, and *z*–*z*′ (Figs 6 and 7).

Downloaded from http://gji.oxfordjournals.org/ by guest on January 7, 2015

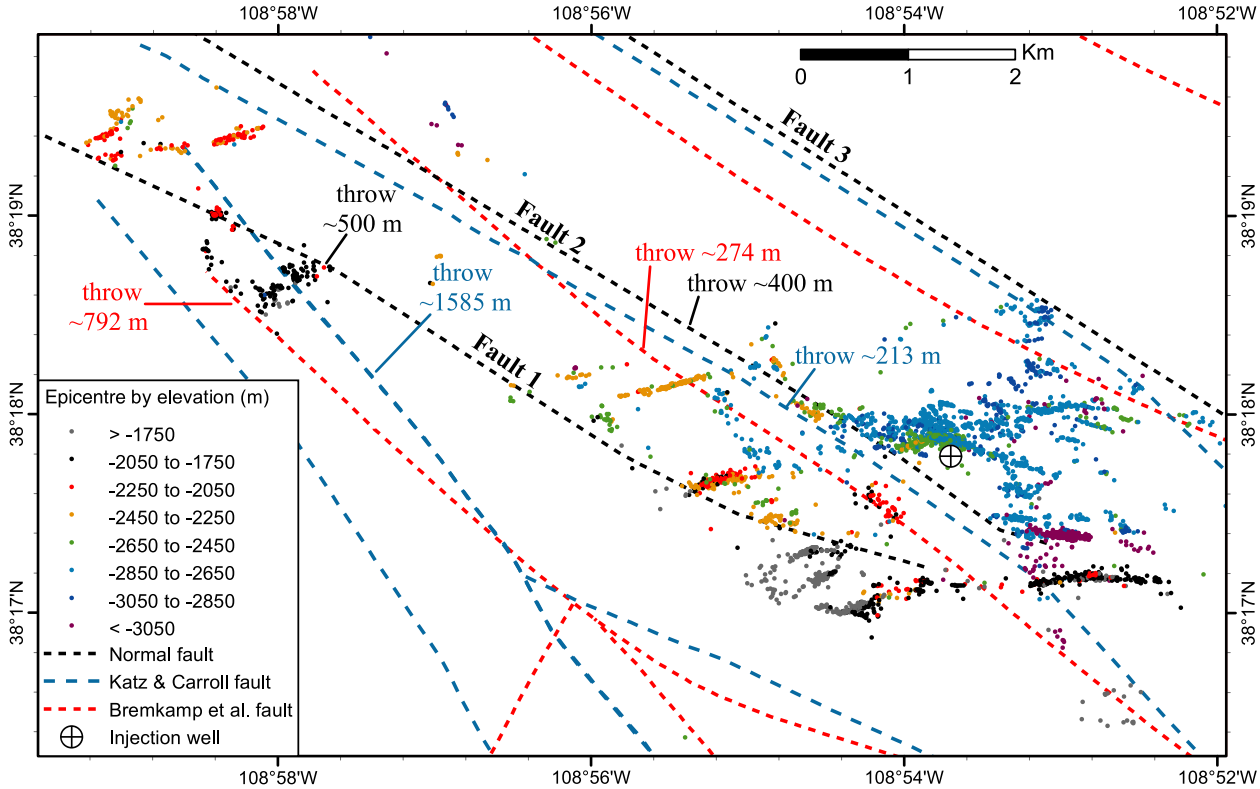

Figure 8. Comparison of the normal faults interpreted from the hypocentre elevation patterns to those interpreted from deep seismic reflection data by Katz & Carroll (1984) and Bremkamp *et al.* (1984). The approximate throws across faults 1 and 2 from each interpretation are indicated on the map. Only a-quality hypocentres from the event relative location are shown.

A comparison of the locations and offsets of the faults inferred from the hypocentre elevations to those interpreted from the seismic reflection data shows both similarities and differences (Fig. 8). Bremkamp *et al.* (1984) and Katz & Carroll (1984) both interpreted a northwest-striking normal fault just southwest of the injection well. Our revised model places this normal fault (Fault 2) 200–500 m closer to the well than their interpretations. We infer a throw of roughly 400 m for this fault. A smaller throw was determined from the seismic reflection data: Bremkamp *et al.* interpreted a throw of about 274 m, while Katz and Carroll indicate a variable throw ranging from about 122 to 305 m, corresponding to an average value of 213 m. Both groups of previous investigators interpreted at least one additional normal fault to the southwest. Their interpretations place the northwest end of these faults in or near the NW cluster and within about 500 m of our Fault 1 (Fig. 8). However, they interpreted these faults to have a more northerly orientation than our interpreted Fault 1, and they do not pass through the near-well region of induced seismicity as Fault 1 does. Our interpreted throw for Fault 1 ranges from 500 to 900 m. We consider a throw of 500 m to be more likely given the observations in cross-section x–x' (Fig. 6). Bremkamp *et al.*'s interpreted throw is between our two estimates but closer to the upper value: 792 m. Katz and Carroll's interpreted throw is substantially higher than either of our estimates: 1585 m.

Bremkamp *et al.* (1984) interpreted two pillow-type Paradox salt features southwest of the injection well, and the location of our inferred strike-slip fault in model 1 corresponds to the saddle between these features (Fig. 9). Hence, if this strike-slip fault does exist, movement along this fault may have contributed to the development of the present-day salt configuration.

Dozens of earthquakes (magenta symbols) have occurred around the northern edge of the southern salt pillow (labelled 'II' in Fig. 9). These events have anomalously shallow hypocentres (mostly above −1250 m elevation) and occur above the interpreted top of the Paradox salt. These seismic events have somewhat different characteristics than those occurring deeper: they occur infrequently and generally not in swarms, their magnitudes tend to be small (mostly $\leq M_D$ 1.5), and their epicentres are dispersed rather than tightly clustered. Most will not tie into the event relative location procedure, even when one or two of these events are chosen as fixed events, suggesting that their waveforms are not only dissimilar to the deeper events but also to each other. The occurrence of earthquake swarms and multiplets of events having similar waveforms is often associated with fluid flow and increasing pore pressure (Baisch & Harjes 2003). The lack of such characteristics in the shallow events and their occurrence above the confining salt layer suggests that they may not be induced by direct pore pressure increase from injection. An alternative explanation is that these earthquakes are triggered by transfer of stress from mechanical deformation of the reservoir. Occurrence of shear-slip seismic events in the overburden in the absence of pore pressure perturbation has been demonstrated in mechanical modelling studies and suggested as an explanation for shallow seismicity associated with CO_2 injection (Angus *et al.* 2010; Verdon *et al.* 2011). In addition, the complex stress and pore pressure patterns in formations adjacent to salt bodies (Fossum & Fredrich 2002; Luo *et al.* 2012; Nikolinakou *et al.* 2012) could make the area around the salt pillow more susceptible to experiencing induced seismicity from stress transfer than other regions.

Downloaded from http://gji.oxfordjournals.org/ by guest on January 7, 2015

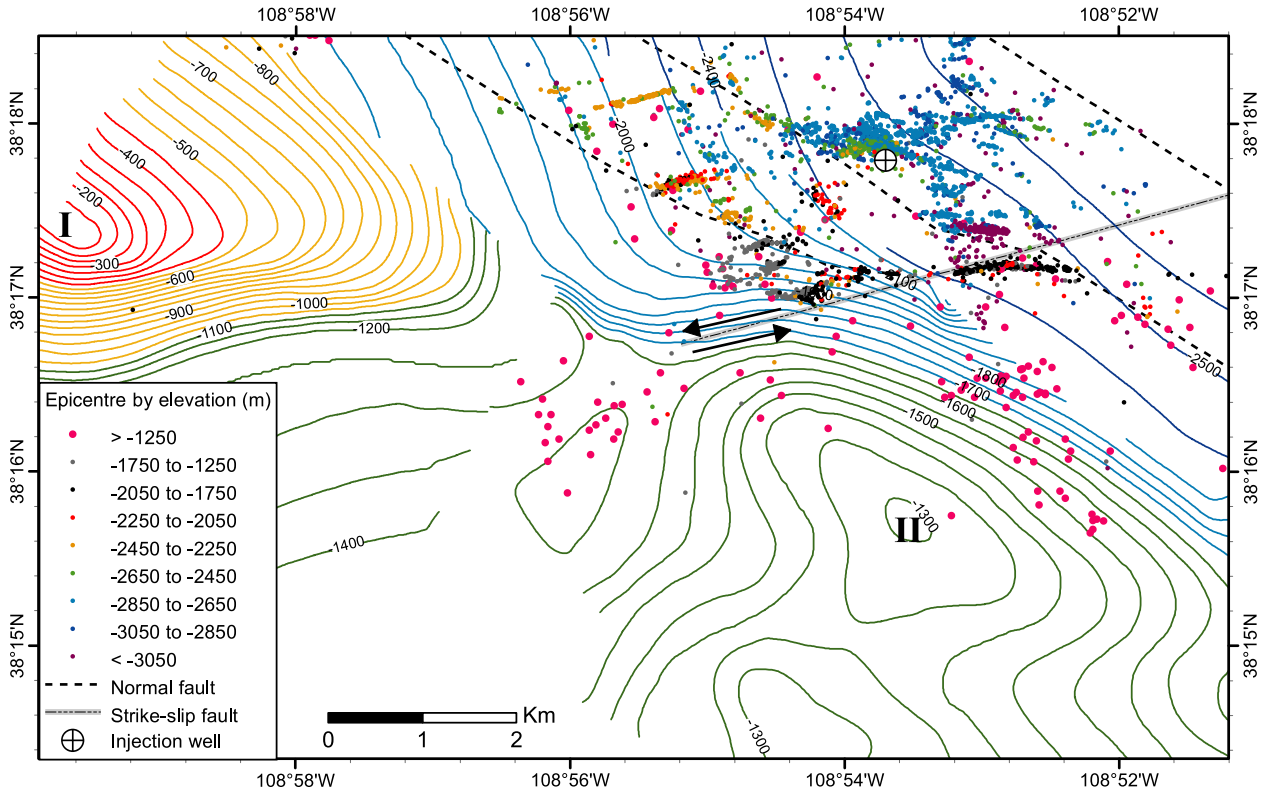

Figure 9. Contours of the top of the Paradox formation massive salt member from Bremkamp *et al.* (1984) and epicentres of induced earthquakes colour-coded by hypocentre elevation. All earthquake epicentres (a- and b-quality) are included. Contour values are elevations in metres relative to mean sea level. Contours were originally drawn in feet, and were digitized, interpolated, and recontoured with a contour interval of 50 m. The labels 'I' and 'II' identify the two salt pillows discussed in the text.

Spatiotemporal epicentre patterns

From the spatiotemporal pattern of epicentres of events induced in the near-well area, we infer the presence of two orientations of large-scale conjugate fractures, which we denote as fracture orientations *A* and *B*. Epicentre lineations along a third direction, which we denote as *C*, are observed near the injection well. Initially, we examine the spatial distribution of epicentres as they evolve over time to infer these orientations and do not assume that slip direction is necessarily parallel to the epicentre lineations. We illustrate the spatial evolution of seismicity along the inferred fracture orientations with the series of cumulative time maps of near-well seismicity shown in Fig. 10.

The initial distribution of epicentres of earthquakes recorded during and after injection tests conducted between July 1991 and June 1994 is shown in Figs 10(a) and (b). Over this time period, epicentres begin to spread out along an axis trending ∼N75°W, subparallel to the estimated direction of maximum horizontal stress, $S_{H\max}$, reported previously (N70°W; Ake *et al.* 2005). The epicentres of initial events may occur along this preferred orientation because pre-existing fractures aligned subparallel to the direction of maximum horizontal stress are more likely to dilate and accommodate fluid flow, or because the lineations simply reflect the orientation of pre-existing fractures and concurrent slip directions. In either case, new fractures created near the injection well (hydrofractures) should tend to align subparallel to the direction of maximum horizontal stress, therefore enhancing preferential fluid flow in that direction (Lee & Ghassemi 2010).

Beginning in the second half of 1994 (Fig. 10c), we see new earthquake epicentres begin to align along two orientations that we interpret to correspond to pre-existing conjugate fracture sets. In the plots, we label one set of inferred fractures set *A* (fractures A1, A2, etc.) and the other set *B*. Initially, several small linear groupings of epicentres are observed near the well, which trend about N31°W and correspond to fracture set *B* (Fig. 10c). There is also a single linear grouping of epicentres near the well which trends approximately N77°E, corresponding to fracture set *A*. Over time, as more fluid is injected and increased pore pressures expand away from the well, the pattern of earthquake epicentres aligning in orientations *A* and *B* becomes increasingly clear (Figs 10d–i). We do not attempt to label every epicentre lineation, but only the most obvious or largest-scale features that become evident during each time period shown. This method is by nature subjective, but regardless of how many distinct fractures we interpret, earthquake clusters appear to align primarily along the *A* and *B* orientations.

In addition to the groupings of epicentres along the *A* and *B* orientations, epicentre lineations exhibiting a third orientation, ∼N71°W, occur near the well (Figs 10c–i). We label this orientation *C*. An epicentre lineation with orientation *C* develops at the deviated wellbore as early as 1994 (fracture C1, Fig. 10c). Additional small-scale epicentre lineations with the *C* orientation appear north and east of the injection well in subsequent years (Figs 10e–i).

In the above analysis, we identify possible fractures based solely on the spatial distribution of precise relative earthquake hypocentres. This approach is feasible for our case because focal mechanism analysis indicates that most faulting is strike-slip on near-vertical planes (Ake *et al.* 2005), because many of the active fractures are widely spaced, and because much of the seismicity appears to occur

Downloaded from http://gji.oxfordjournals.org/ by guest on January 7, 2015

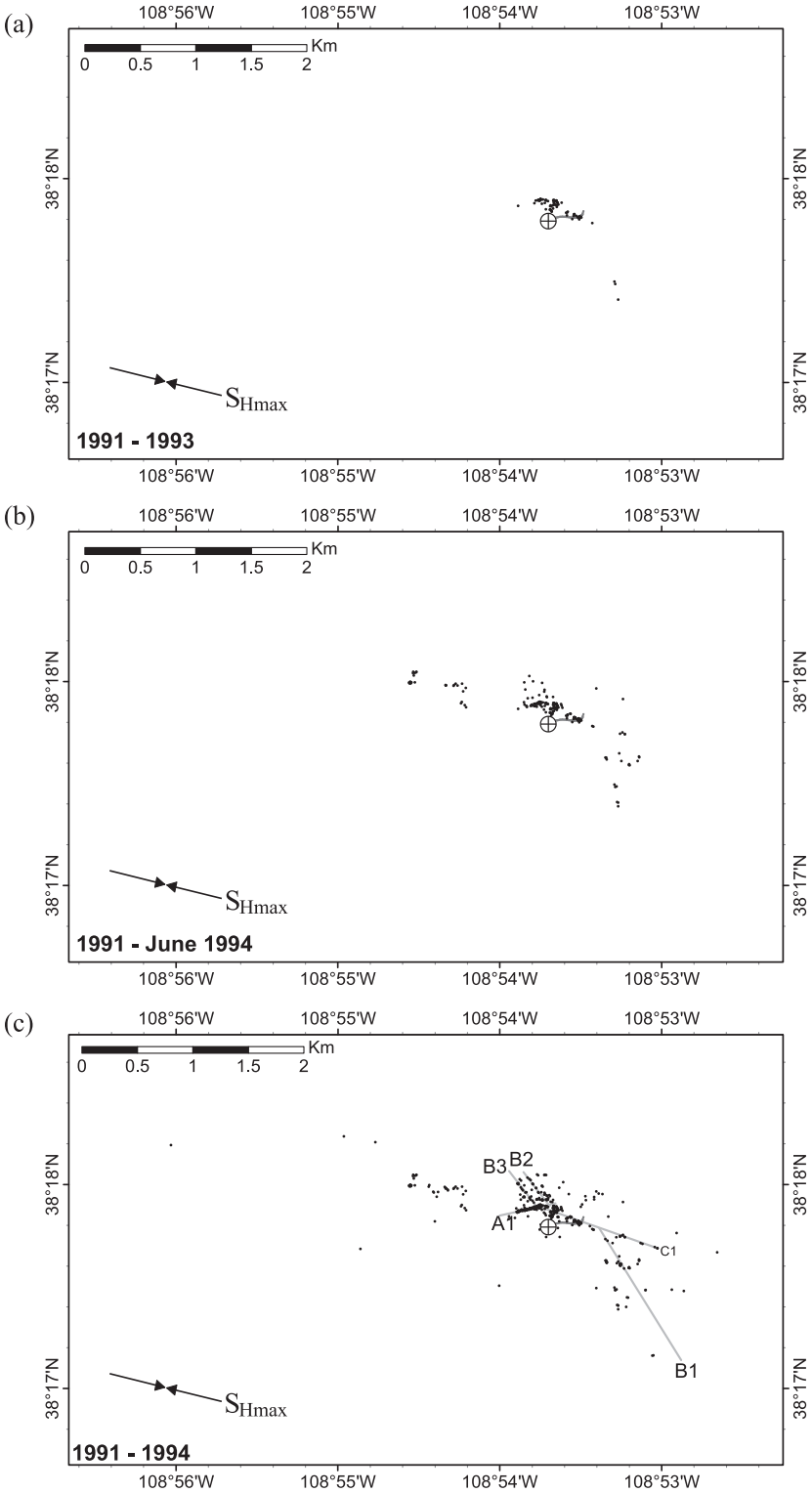

Figure 10. Maps showing a-quality epicentres of PVU-induced events occurring in the near-well region cumulatively over time: (a) 1991–1993; (b) 1991–June, 1994; (c) 1991–1994; (d) 1991–1996; (e) 1991–1997; (f) 1991–June, 1998; (g) 1991–1998; (h) 1991–1999; and (i) 1991–2013. The grey lines indicate linear trends that appear to control the spatial expansion of seismicity over time.

within or near the target injection formations. Results from a new focal mechanism analysis discussed in the following section indicate that fault slip is consistent with the observed orientations of the epicentre lineations. Other types of analyses based on waveform similarity, such as multiplet clustering techniques that have been applied at other sites of induced seismicity (Baisch & Harjes 2003; Moriya *et al.* 2003), may prove useful for determining finer-scale features within the general model presented here.

Downloaded from http://gji.oxfordjournals.org/ by guest on January 7, 2015

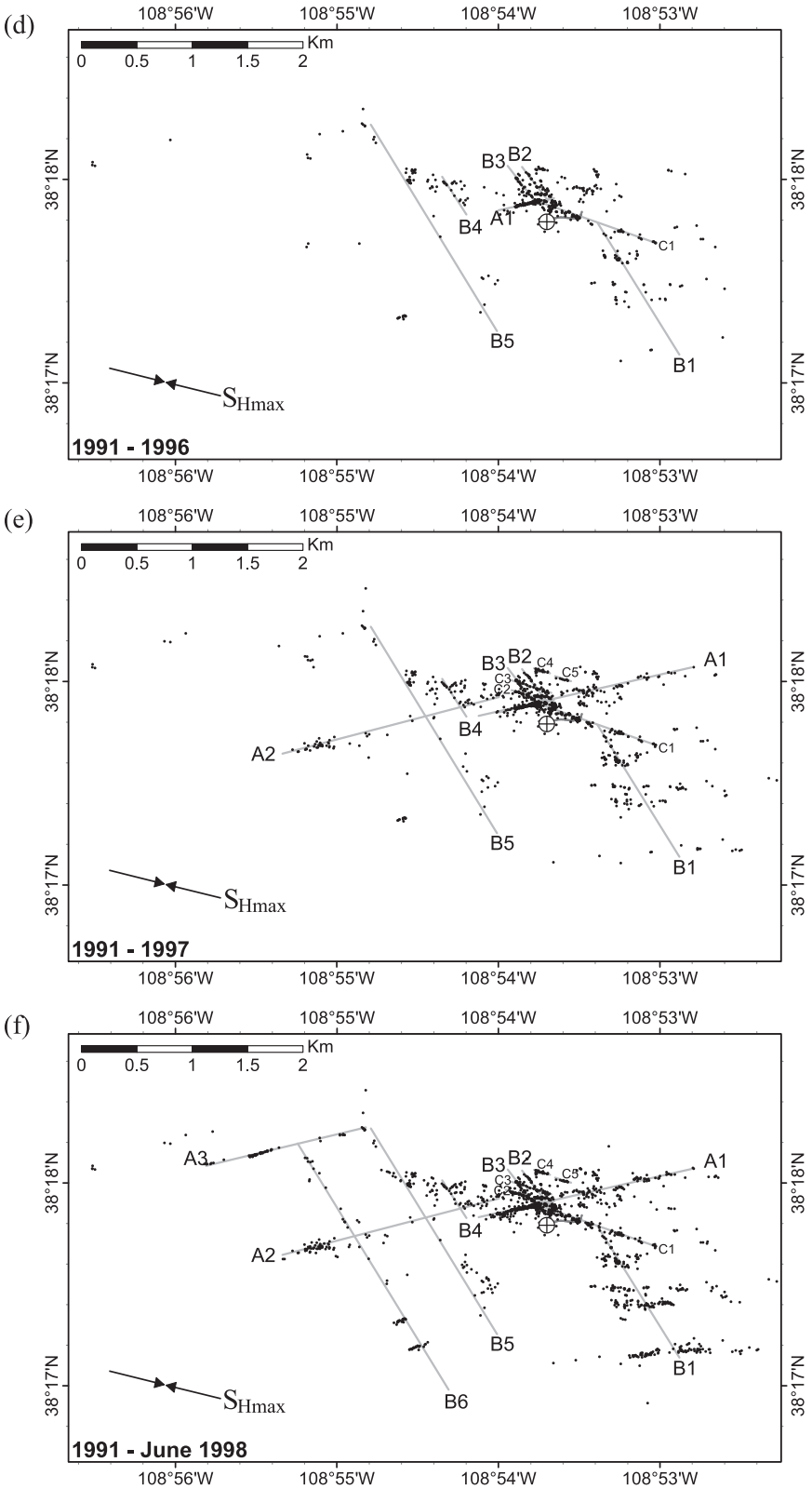

Figure 10. (*Continued.*)

Downloaded from http://gji.oxfordjournals.org/ by guest on January 7, 2015

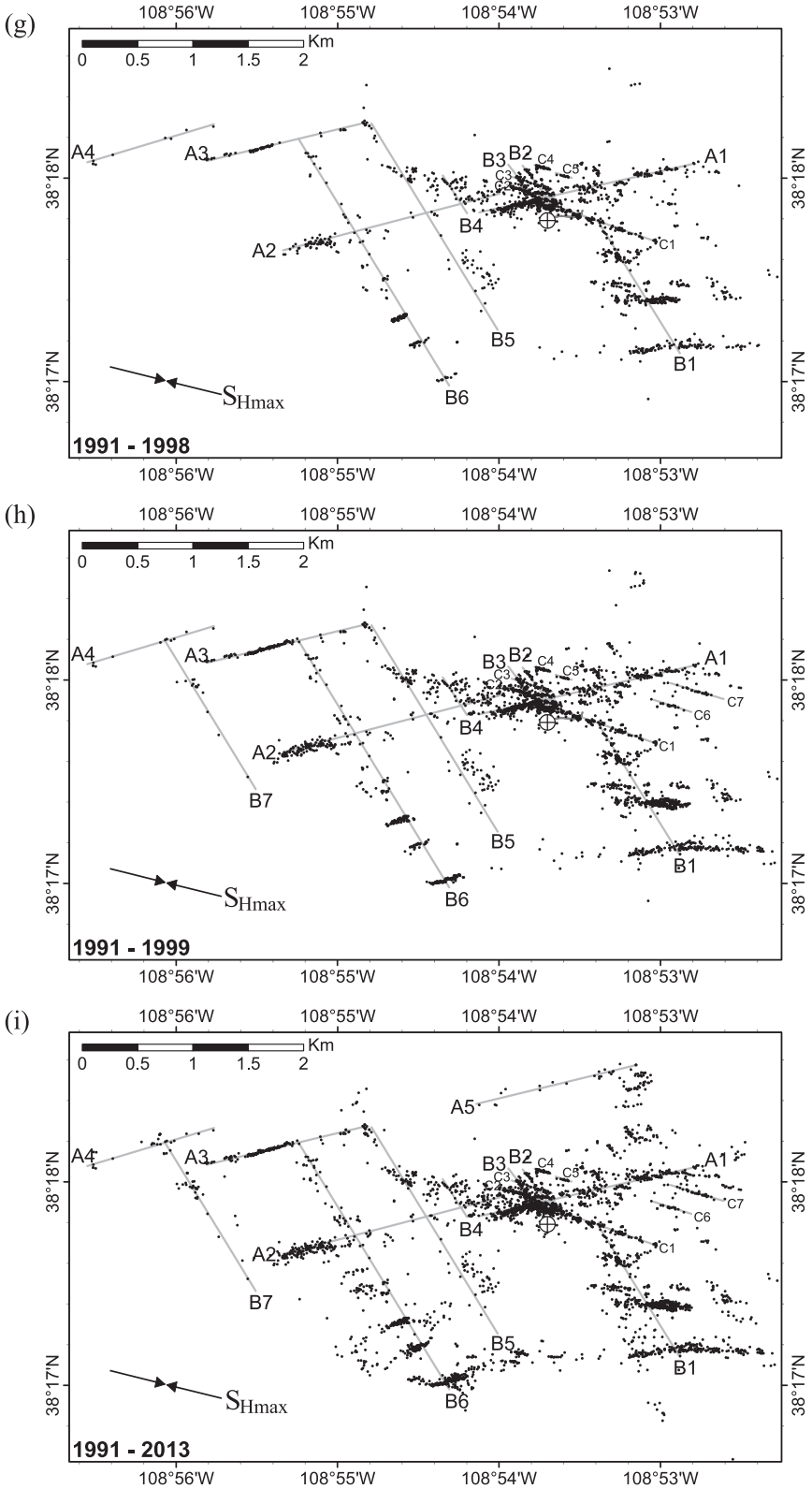

Figure 10. (*Continued.*)

Downloaded from http://gji.oxfordjournals.org/ by guest on January 7, 2015

FOCAL MECHANISM AND STRESS ANALYSES

Focal mechanism results

Results from a new analysis of focal mechanisms provide additional constraints on the fracture model presented above. Previous work on focal mechanisms had indicated that events in the near-well region and NW cluster were predominantly strike-slip, with a preferred fault orientation roughly corresponding to the orientation of fracture sets *A* or *B* (Ake *et al.* 2005; Block *et al.* 2014). Ake *et al.* (2005) found that 89 per cent of the roughly 1300 focal mechanisms they studied were strike-slip; of these, 86 per cent had a preferred fault plane strike in the ENE direction (average N86°E), and the remainder had a preferred fault plane strike in the NW direction (average N49°W). Block *et al.* (2014) found a preferred strike direction of N78°E for an M_L 4.4 earthquake in the NW cluster, which agreed well with the trend of epicentres from aftershocks of that earthquake.

We reanalysed approximately 600 earthquakes with a-quality locations in the near-well area, the northwest cluster, and the southeast cluster. As part of this analysis, *P*-wave first breaks at all stations were manually repicked, and focal mechanisms were determined using the *FOCMEC* computer code (Snoke 2009) using azimuths and take-off angles determined from our 3-D velocity model. Our preliminary focal mechanisms are determined using only vertical-component *P*-wave first motion data, and do not yet incorporate body wave amplitudes or *S*-wave polarities to provide additional constraints. Gaps in PVSN station coverage prior to 2011 result in substantial uncertainty in the computed focal mechanisms for many earthquakes. Most PVU-induced earthquakes occurred in 1999 or before, when PVSN consisted of just 15 stations, only one of which was within a focal depth of the injection well. Two additional close-in stations were installed in June 1999 and November 2005, and the network was substantially upgraded in 2011 to add five new stations (two distant stations were decommissioned). Focal mechanisms for the post-2005 data typically are better constrained than for the earlier data.

Our new analysis confirms the observations from earlier studies that most focal mechanisms are strike-slip (83 per cent), have a *P*-axis oriented to the northwest, have a *T*-axis oriented to the northeast, and have one fault plane consistent with the orientations of the epicentre lineations in which the events occur. Many events for which focal mechanisms could be determined occur on small-scale ENE or ESE trending epicentre lineations (Fig. 11). In most cases, these events have strike-slip mechanisms, and the strike of one of the near-vertical nodal planes matches the trend of the corresponding epicentre lineation within 10°. We therefore identify these nodal planes as the likely fault planes. Fig. 11 shows the spatial distribution of the presumed fault plane strikes for the near-well area, the NW cluster, and the SE cluster. Over much of this area, the strikes of the presumed fault planes approximately coincide with the fracture set *A* orientation determined from epicentre lineations (N77°E) (red fault planes in Fig. 11). These fault planes comprise 57 per cent of all strike-slip focal mechanisms, and their average strike is N70°E. In contrast to the fracture set *A* orientations, a N71°W orientation of epicentre lineations, fracture set *C*, is observed in the area east of the injection well (Fig. 11). The average strike of presumed fault planes from the focal mechanism analysis in this area is N77°W, and these events comprise 29 per cent of the strike-slip mechanisms (blue fault planes in Fig. 11). Fracture set *C* is rotated 32°

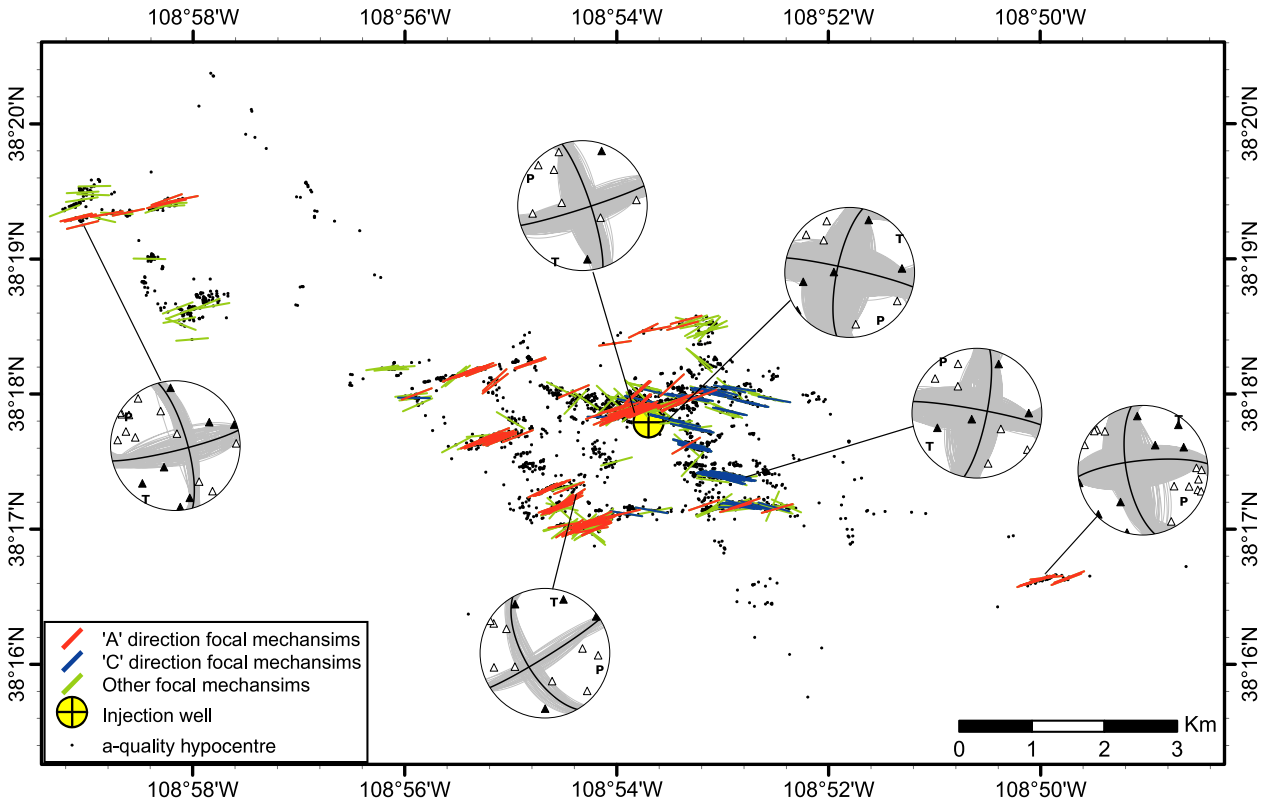

Figure 11. Strikes of favoured fault planes classified by direction, including 'A' direction events (red), 'C' direction events (blue) and unclassified events (green). Example focal mechanism solutions include all possible solutions (grey lines) and preferred mechanisms (black line). Black triangles denote compressional first motions picks and white triangles denote tensional first motion picks. Preferred mechanism's *P*- and *T*-axes are labelled.

Downloaded from http://gji.oxfordjournals.org/ by guest on January 7, 2015

clockwise from fracture set *A*, as determined by epicentre lineations, and 33° as determined by focal mechanisms. Assuming that the nodal plane whose strike most closely matches the trend of the epicentre lineations is the actual fault plane, the presumed fault planes for both fracture sets *A* and *C* are indicative of right-lateral slip.

Focal mechanisms consistent with fracture sets *A* and *C* appear to be segregated by area and by focal depth. Focal mechanisms and epicentre lineations oriented in the *C* direction are common in the area immediately east and southeast of the injection well, but few focal mechanisms consistent with fracture set *A* have been identified in this area (Fig. 11). Similarly, focal mechanisms and epicentre lineations consistent with fracture set *A* are abundant in the area immediately west of the injection well and in more distant seismicity clusters, but focal mechanisms and epicentre lineations consistent with fracture set *C* are not present in these areas. In the area close to the injection well, hypocentres of events with focal mechanisms oriented in the *A* direction generally are a few hundred metres shallower than those of events oriented in the *C* direction. For example, Fig. 12 shows the time and depth evolution of events with focal mechanisms; hypocentres from a cluster of *A*-oriented events in 1998–1999 immediately northwest of the injection well are at elevations of −2250 to −2650 m, while clusters of *C*-oriented events observed immediately east of the injection well during the same period are at elevations of −2650 to −2850 m. In general, the trends of epicentre lineations and focal mechanisms have been consistent over the time since injection operations began, as indicated by Fig. 12. The local state of stress within a reservoir can change spatially or temporally, either from variations in lithology or changes in the local strain tensor, particularly if the material is anisotropic (Bruno & Winterstein 1994). The focal mechanism trends shown in Fig. 12 suggest that the apparent change in stress indicated by fracture sets *A* and *C* is likely related to pre-existing geological structure, although we cannot rule out injection-induced anisotropy that may have occurred early in the injection and which has since remained relatively constant as a possible cause.

It is possible that some or all of the events that we have associated with fracture set *A* are instead occurring on the conjugate nodal planes approximately oriented in the direction of fracture set *B*. In contrast to fracture set *A* (N77°E), we have largely inferred the existence of fractures in set *B* (N31°W) from the larger-scale alignments of clusters of epicentres (Fig. 10), since few distinct epicentre lineations are parallel to the strike of fracture set *B*. The average trend of strike-slip nodal planes approximately in the fracture set *A* direction is N70°E; the average trend of the conjugate nodal planes is N19°W. There is a difference of about 7° between the trend of fracture set *A* as determined from epicentre lineations and the average of the presumed fault planes for events with compatible focal mechanisms. If instead the conjugate nodal planes of these events are considered to be the fault planes, then the difference between the average strike of the conjugate planes and the orientation of fracture set *B* (as determined from epicentre lineations) is somewhat greater, about 12°. Thus the nodal planes with strike in the fracture set *A* direction are in better agreement with fracture orientations inferred from epicentre lineations than the conjugate planes with strike in the fracture set *B* direction. Given the uncertainty in the individual focal mechanism solutions we cannot preclude that some of these events are consistent with faulting on fracture set *B*. However, the greater misfit found when associating nodal planes in the fracture set *B* direction is consistent with the stress model discussed in the following section.

We also considered the limits that the focal mechanism data place on a single uniform regional stress that could produce slip on both fracture sets *A* and *C*. Focal mechanisms constrain the local direction of maximum compressive stress σ_1 to be within the nodal plane quadrant containing the *P*-axis (McKenzie 1969). Given the consistency of the focal mechanisms with *A* or *C* orientations, which indicate predominantly strike-slip motion, then under the assumption of a single uniform regional stress and isotropic materials, the σ_1 direction must fall within the intersection of the average *P*-axis quadrants of both sets, which is the azimuth range of approximately N19°W to N77°W. To provide further insight into the most likely σ_1 direction under these assumptions, we performed stress inversions of the focal mechanisms for two cases: (1) assuming that either nodal plane could be the fault plane and (2) assuming that the nodal plane which has a strike closest to 90°, and therefore is closest to either the *A* or *C* fracture direction, is the fault plane. To perform the stress inversion, we used the *SATSI/MSATSI* computer codes (Hardebeck & Michael 2006; Martínez-Garzón *et al.* 2014). These calculations yielded mean σ_1 directions of N54°W and N55°W for the two cases, respectively. As discussed in the following section, if the formation properties are isotropic, then this stress direction appears to be incompatible with contemporaneous slip on both fracture sets *A* and *C* for reasonable values of internal friction.

Stress models

Interpreting fracture sets *A* and *B* as sets of conjugate near-vertical shear fractures leads to an inferred direction of maximum horizontal stress at the time of fracture development of ∼N67°W (the angle bisecting orientations *A* and *B*). This inferred direction of maximum horizontal stress is consistent with previously reported *P*-axes of focal mechanisms of near-well PVU-induced earthquakes of N64°W to N67°W (Ake *et al.* 2005). The angle between the inferred stress direction of N67°W and the strike of either set of fractures is 36°, somewhat larger than the typical 30° angle for brittle shear fracturing (Singhal & Gupta 2010). Assuming a Mohr–Coulomb fracture criterion, the observed fracture angle indicates a corresponding coefficient of internal friction of ∼0.3, which would represent an average, or effective, coefficient for all the formations in which the fracturing originally occurred.

The current direction of maximum horizontal stress in the vicinity of the PVU injection well is not well constrained from available data. Data from the World Stress Map Project indicate that the current direction of regional maximum horizontal stress has a more westerly orientation than that present when the conjugate fracture sets developed. Three of the four reported stress measurements within 150 km of the PVU injection well have maximum horizontal stress directions between N77°W and N79°W, based on focal mechanism analyses (Heidbach *et al.* 2008). In contrast, the inversions of focal mechanisms of PVU-induced events described in the previous section indicate a more easterly orientation for $S_{H\max}$, ∼N55°W. Previous breakout analysis of televiewer data acquired in the lower section of the PVU wellbore (at and below the Leadville formation) indicates a direction of $S_{H\max}$ of ∼N84°W (personal communication from Steve Hickman and Robert Summers, U.S. Geological Survey, Menlo Park, CA, 2003). However, a comparison of borehole long-axis azimuths from the televiewer and dipmeter logs shows a discrepancy of 30°, with the dipmeter log suggesting a corresponding $S_{H\max}$ direction of ∼N54°W.

To investigate the compatibility of different directions of $S_{H\max}$ with observed epicentre and focal mechanism patterns of PVU-induced seismicity, we examine the stress condition required for

Downloaded from http://gji.oxfordjournals.org/ by guest on January 7, 2015

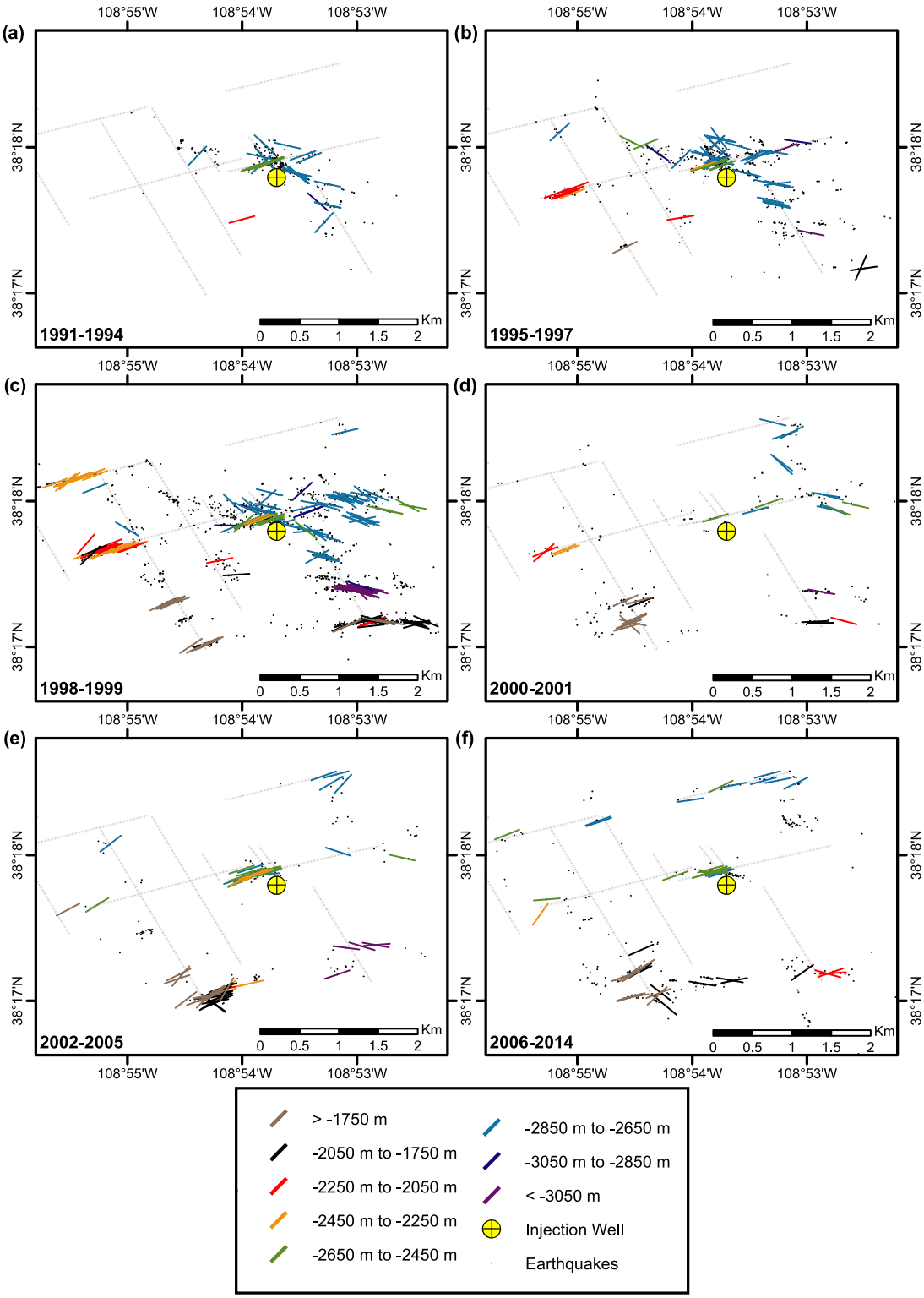

Figure 12. Time and depth evolution of focal mechanisms. Time windows include: (a) 1991–1994; (b) 1995–1997; (c) 1998–1999; (d) 2000–2001; (e) 2002–2005; (f) 2006–2014. The strike of the preferred fault plane is shown as a solid line, coloured by depth interval. Grey dotted lines denote observed linear epicentre trends, as in Fig. 10. A-quality hypocentres are shown as black dots.

slip on a pre-existing (vertical) fracture in isotropic rock (Scholz 2002):

$$\frac{\sigma_1 - p}{\sigma_3 - p} = \frac{1 + \mu \cot(\theta)}{1 - \mu \tan(\theta)}, \tag{1}$$

where σ_1 is the maximum stress, σ_3 is the minimum stress, p is pore pressure, θ is the angle between the direction of σ_1 and the strike of the pre-existing fracture, and μ is the coefficient of internal friction. In the case of a vertical fracture, σ_1 corresponds to the maximum horizontal stress, $S_{H\max}$. We calculate the right-hand side of this

Downloaded from http://gji.oxfordjournals.org/ by guest on January 7, 2015

equation as a function of θ. We then examine the values of the stress ratio curve corresponding to the angles (θ) for fracture orientations *A*, *B* and *C*, for each assumed direction of $S_{H\max}$. This analysis indicates the relative likelihood for fractures with orientations *A*, *B* and *C* to experience shear slip for each stress model. Comparison of the results with the observed faulting patterns of PVU-induced events is then used to evaluate the different stress models.

The appropriate value to use for the coefficient of internal friction, μ, is not well constrained by available data. The value inferred from the angle between fracture sets *A* and *B* (0.3) may not be appropriate. Rock properties and confining stress likely have changed since the fractures first developed. Also, the coefficient of internal friction derived from the fracture angles represents an effective value, likely influenced by properties of multiple formations and rock types. In contrast, we interpret PVU fluid injection to be preferentially reactivating the portions of the fractures within the Leadville limestone. Because of these uncertainties, we compute the stress condition using a range of values of μ reported for limestones: 0.4–0.8 (Clark 1966). For easier comparison, we normalize each curve by its minimum value.

We compute θ values for three stress models, corresponding to the maximum horizontal stress direction from the World Stress Map data (N78°W, Fig. 13a), the stress direction obtained from our focal mechanism analysis (N55°W, Fig. 13b), and an optimal stress direction for slip on fracture set *C* (N45°W, Fig. 13c). Each figure shows a range of angles for fracture sets *A*, *B* and *C*, as indicated by the shaded areas. The bounds of the shaded areas are determined from the orientations of the epicentre lineations (thick vertical lines) and the strikes of the presumed focal mechanism fault planes (thin vertical lines) for each fracture set.

Under the assumption that the direction of regional $S_{H\max}$ from the World Stress Map data applies to PVU, fracture set *A* is preferentially oriented for slip, whereas fracture set *B* requires a greater increase in pore pressure for slip (Fig. 13a). This is consistent with the relative numbers of epicentre lineations and focal mechanisms compatible with these orientations observed for PVU-induced seismicity. Furthermore, the observed right-lateral slip on fractures in set *A* is consistent with this stress direction. In this stress model, fractures with orientation *C* are very unlikely to experience shear slip, and therefore this model is not consistent with the epicentre lineations and focal mechanisms with the *C* orientation observed near the injection well. In addition, set *C* fractures would experience left-lateral strike-slip movement under this stress model, whereas right-lateral movement is observed.

If the single regional stress direction obtained from inversion of the PVU focal mechanism data is correct, then fracture set *B* is very favourably oriented for shear slip and fracture set *C* is also fairly favourably oriented for slip (Fig. 13b). In contrast, slip on fracture set *A* would require either a relatively low value of internal friction, 0.4 or less, or a high pore pressure perturbation. The observed right-lateral slip on fractures in set *C* is consistent with this stress direction. This model is consistent with the shear slip observed on set *C* fractures near the injection well. However, it is not consistent with the lack of epicentre lineations in the *B* direction in all areas or with the abundance of observed epicentre lineations and focal mechanisms with the *A* orientation in areas away from the well.

Finally, if a hypothetical N45°W stress direction optimal for slip on fracture set *C* is assumed, then slip is somewhat favorable on fracture set *B*, but very unfavourable for slip on fracture set *A* (Fig. 13c). This model is consistent with observations of epicentre lineations and focal mechanisms in the area near the injection well but is not consistent with patterns observed farther from the well.

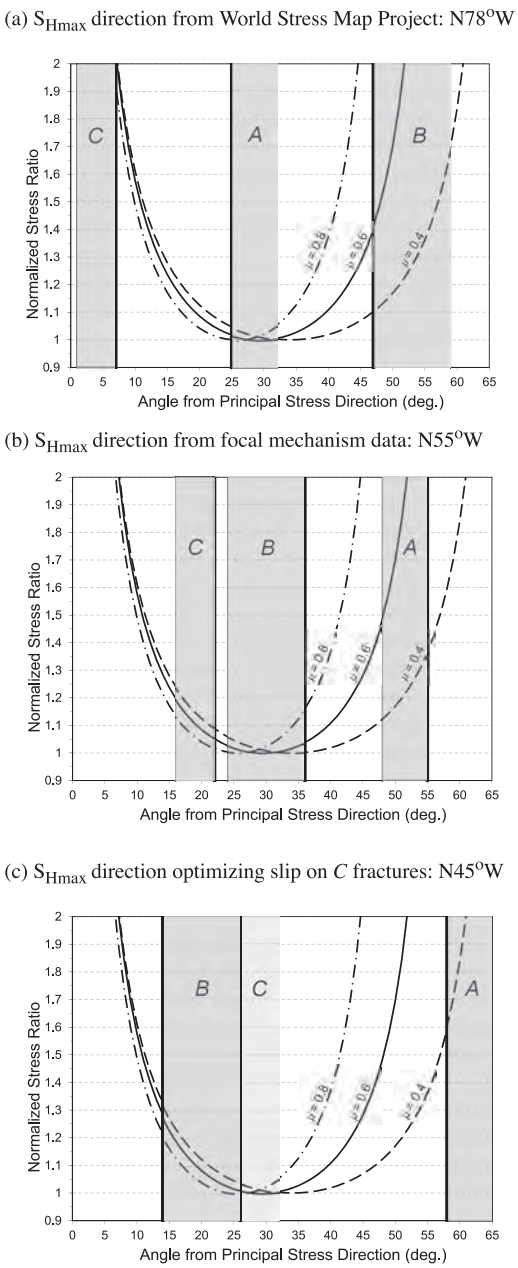

Figure 13. 2-D stress conditions required for slip on a pre-existing fracture as a function of the angle of the fracture from the principal stress direction. Results for three different values of the coefficient of internal friction are shown ($\mu = 0.4$, 0.6 and 0.8), with each curve normalized by its minimum value. The shaded areas show the range of angles for fracture sets *A*, *B* and *C*, for three different estimates of the maximum stress direction. The thick and thin vertical lines correspond to angles computed from orientations of epicentre lineations and focal mechanism solutions, respectively.

Under the assumption of isotropic materials, it does not appear that a uniform stress direction can meet conditions necessary for slip on both fracture sets *A* and *C*, nor can a single stress direction explain the relative abundance of events falling into the corresponding epicentre and focal mechanism classes. The direction of regional $S_{H\max}$ from the World Stress Map data is consistent with the preferential shear slip on fractures with orientation *A* (and absence of slip on fractures with orientation *C*) observed for most areas away from the injection well. In contrast, conditions favourable for shear slip on fracture set *C*, which is observed clearly only within

Downloaded from http://gji.oxfordjournals.org/ by guest on January 7, 2015

a limited area adjacent to the well, require the direction of local $S_{H\max}$ to be rotated 30°–35° clockwise from the regional trend. Fracture set *C* is subparallel to the regional $S_{H\max}$ direction, and the sense of slip determined from focal mechanisms is inconsistent with the regional $S_{H\max}$ direction. An $S_{H\max}$ direction of approximately N45°W would be consistent with the right-lateral shear slip on fracture set *C* inferred from focal mechanisms; however, this puts the *A* fractures at an unfavourable orientation for slip. Hence, it appears that two different local stress conditions are required to explain the observed focal mechanisms and epicentre lineations, with the two conditions having a roughly 30°–35° difference in direction of $S_{H\max}$.

As discussed previously, fracture orientations *A* and *C* appear to be segregated primarily by focal depth and by geographic location, but not obviously by time. Spatial variations in stress can arise either from variations in lithology or from changes in the local strain tensor (Bruno & Winterstein 1994). Even with uniform regional strain directions, local variations in the orientation of stress can result from inherent or stress-induced anisotropy, which in turn can arise from different formation stiffness parallel and perpendicular to bedding, unconformities in dip, non-uniform formation thickness and oriented fractures (Bruno & Winterstein 1994). Depth-dependent changes in the azimuth of maximum horizontal stress have been reported in hydrocarbon extraction (Herwanger *et al.* 2013) and geothermal fluid injection (Martinez-Garzon *et al.* 2013). Analysis of the 3-D spatial patterns and temporal variations in focal mechanisms is ongoing and may provide additional insights into possible local stress variations related to injection.

REVISED GEOLOGICAL MODELS

Based on the analyses described above, we propose revised subsurface geological models for the area surrounding the PVU injection well (Fig. 14). Examination of spatial epicentre patterns in areas beyond the near-well region of induced seismicity (>5 km from the injection well) indicates the existence of additional epicentre lineations with orientations similar to those of interpreted fracture orientations *A* and *B*. These are observed in the NW cluster, SE cluster, and one of the northern-valley clusters (Fig. 14a). Hence, fracture orientations *A* and *B* appear to be present over a widespread area within Palaeozoic formations older than the Paradox salt. Since we interpret that the majority of the induced seismicity is occurring below the salt confining layer, we do not know if these fracture sets are also present in younger rock units overlying the Paradox formation.

The northeast-trending strike-slip fault in model 1 (Fig. 14a) is parallel to fracture set *A*. In this model, we interpret the strike-slip fault as representing shear slip on one of the fractures in set *A*. Alternatively, there could be a shear zone here with offset across multiple, closely spaced fractures in set *A*. Although we show the northwest-striking normal faults (Faults 1, 2 and 3 in Fig. 14a) as being continuous other than for the offset across this strike-slip fault or shear zone, they may have offsets across some of the other fractures in set *A* that cannot be resolved with the hypocentres recorded to date.

Since fracture sets *A* and *B* cut across the normal faults (Fig. 14), we interpret that fracture sets *A* and *B* developed as conjugate pairs of near-vertical shear fractures after the majority of movement on the normal faults had occurred. Increased movement along the deep northwest-striking normal faults in Paradox Basin began during the late Mississippian Period, when Paradox Basin began rapidly subsiding, and continued into the Pennsylvanian and Permian Periods, and possibly the Triassic Period (Doelling 1998; Grout & Verbeek 1998). Some studies report the greatest subsidence of Paradox Basin as occurring from middle Pennsylvanian to early Permian time (Stevenson & Baars 1986; Trudgill 2011). Therefore, fracture sets *A* and *B* likely formed during or after the late Pennsylvanian-early Permian Periods.

Neither the present-day topography of Paradox Valley nor its gravity signature (Steenland 1962; Friedman *et al.* 1994; Trudgill 2011) suggest lateral offset of the underlying salt anticline in the vicinity of the proposed strike-slip fault in model 1. Hence, if this fault is present, most of the movement along the fault must have occurred prior to the major growth of the salt anticline. Recent work indicates that the greatest growth rate of the Paradox Basin salt anticlines occurred during deposition of the Cutler Formation in Permian time (Kluth & DuChene 2009; Trudgill 2011). Hence, to pre-date most of the upward movement of salt into the anticline underlying Paradox Valley, movement along the strike-slip fault could have occurred during the late Pennsylvanian or early Permian Periods. Northeast-trending basement faults in northern Paradox Basin, with potential late-Palaeozoic strike-slip movement, have been discussed by other researchers (Hite 1975; Stevenson & Baars 1986; Trudgill 2011).

The chronological development of the features in our revised subsurface models is illustrated in simplified form in Fig. 15. Initially, movement occurred along the normal faults during an extensional stress regime in the late Palaeozoic (step 1 in Fig. 15). This extension began after deposition of the Mississippian-age Leadville Formation and may have been most active during middle Pennsylvanian time (Stevenson & Baars 1986; Trudgill 2011). Subsequently, the stress regime changed to a compressional state with a maximum (horizontal) stress direction of about N67°W, and conjugate shear fracture sets *A* and *B* developed (step 2). For model 1, a temporary rotation of the horizontal stresses to a northeast–southwest compressional state is required to produce left-lateral shear slip of the strike-slip fault interpreted from the hypocentre analysis (step 3). (This step is not required for model 2, since it does not include strike-slip fault displacement.) This change in the stress state could have occurred during the Ancestral Rocky Mountain Orogeny, which began in Pennsylvanian time. This tectonic event produced southwest-directed thrust faulting (Kluth & DuChene 2009; Trudgill 2011) and left-lateral motion on east–west-trending strike-slip faults (Thomas 2007) in and near the Uncompaghre Uplift, north and east of Paradox Valley. Subsequently, the stress field returned to a northwest-southeast compressional orientation, with the current regional direction of σ_1 being ∼N78°W. Finally, the increase in pore pressure within the pre-existing fractures due to fluid injection has caused reactivation of some of these features, with a strong preference for right-lateral shear slip along fractures in set *A* in most areas, due to the present-day orientation of the regional stress field (step 4).

DISCUSSION

The revised subsurface geological models that we have interpreted from the hypocentre elevation patterns can explain some of the large-scale spatiotemporal patterns of PVU-induced seismicity that were mentioned earlier in this paper and are investigated in more detail elsewhere (King *et al.* 2014). Specifically, seismicity was first observed in the region of the NW cluster (6–8 km from the well) in mid-1997, just 1 yr after the start of long-term PVU fluid

Downloaded from http://gji.oxfordjournals.org/ by guest on January 7, 2015

(a) Fault model 1

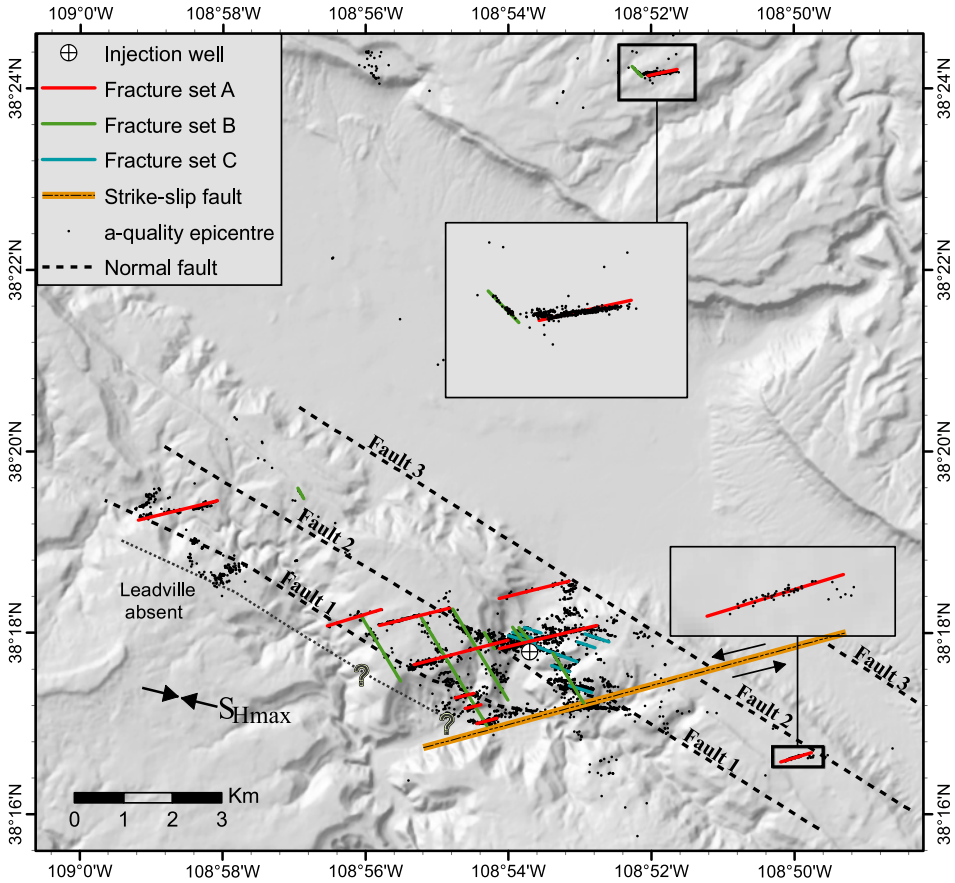

(b) Fault model 2

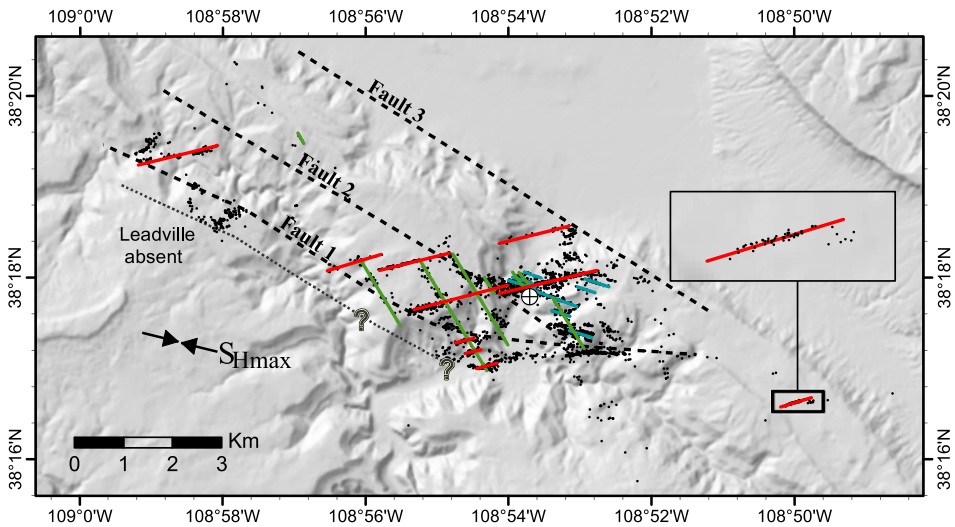

Figure 14. Two proposed deep (subsalt) geological models for the vicinity of the PVU injection well, showing interpreted faults and fracture sets. Fault geometries are approximate.

injection, and distinct clusters of events formed within the following 6 months. In contrast, no seismicity was observed at the location of the SE cluster (∼6 km from the well) until 2004, and a distinct cluster did not develop here until 2010, 14 yr after the beginning of long-term injection. In fact, shallow earthquakes that we interpret as being related to PVU fluid injection were occurring across Paradox Valley, at distances up to 16 km from the injection well, several years prior to seismicity being detected in the SE cluster. These seismicity patterns may be due to the fault geometries south of the injection well. The strike-slip fault in model 1 may act as an impermeable

Downloaded from http://gji.oxfordjournals.org/ by guest on January 7, 2015

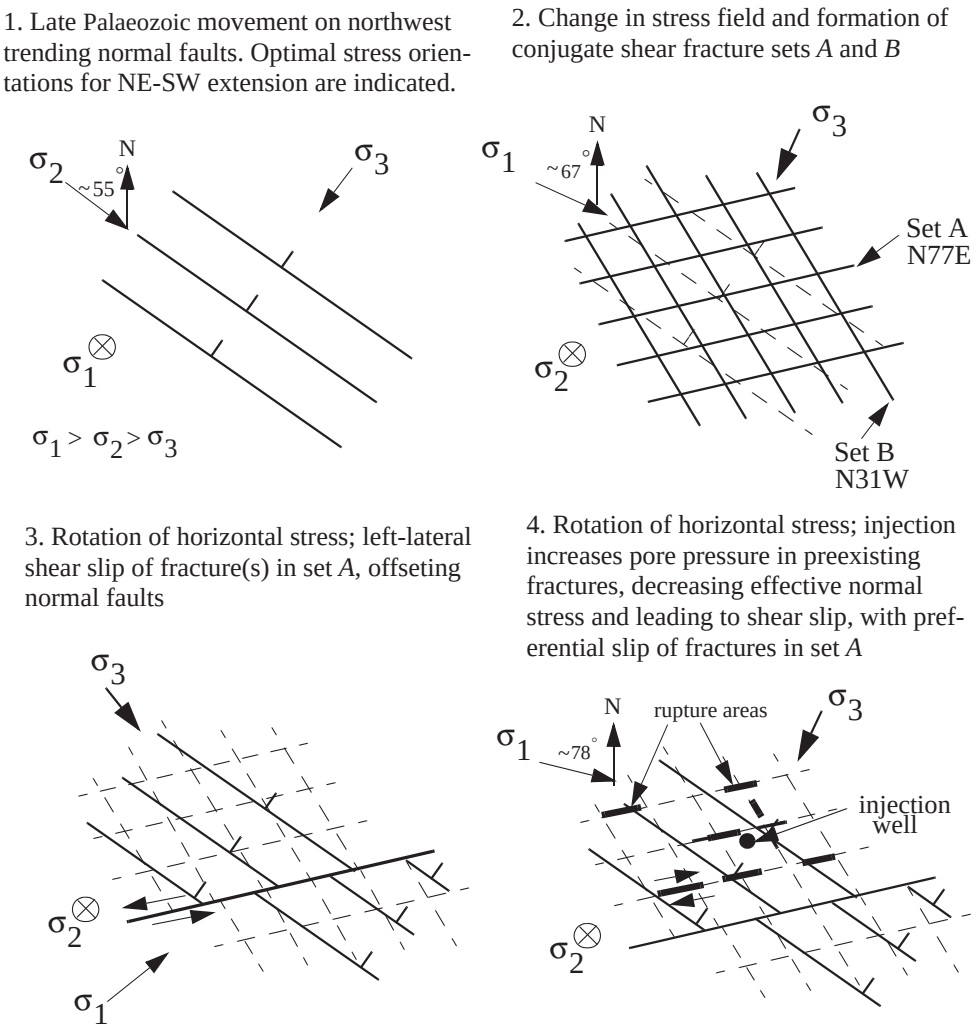

Figure 15. Conceptual chronological development of subsurface structural model. The chronological steps are sequentially numbered and described within the figure. Step 3 is required for fault model 1 (Fig. 14a) but not for fault model 2 (Fig. 14b).

barrier at relatively low pore pressures, and substantial fluid flow and pore pressure propagation may only occur across the fault zone when pore pressures are sufficiently elevated. In model 2, the fault geometry suggests that the SE-cluster events may be occurring within the Precambrian basement. In this case, the delayed onset of seismicity in the SE cluster could be due to lower permeability and corresponding lower flow rate through the Precambrian basement toward the southeast than through the Leadville formation to the northwest.

Knowledge of the subsurface geological structure will be useful in constraining estimates of the maximum magnitude induced earthquake that may occur. A previous PVU study indicates that the magnitude of a large event (M_L 4.4) which occurred in the NW cluster in 2013 corresponds closely to that estimated using the fault segment length delineated by previous seismicity and a circular crack rupture model (Block *et al.* 2014). Hence, the lengths of specific fractures identified in this study, particularly those in set A which are preferentially oriented for slip, could potentially be used to estimate the magnitudes and locations of significant induced earthquakes that may occur in the future. However, an important issue that must first be resolved is whether the vertical offset of the injection target formation across the northwest-striking normal faults may act to inhibit rupture on faults that cross them, such as those in set *A*. Preliminary analysis of the aftershock patterns of the induced earthquakes with local magnitude of 3.5 or greater suggests that this may be the case: that is, aftershock patterns from these events tend to truncate at the northwest-trending normal faults. In this case, earthquake magnitudes would be limited by the length of active fault segments within a single fault block (Blocks 1, 2 or 3).

The revised geological models have implications for the site selection of a potential second PVU injection well. Based on these models, areas surrounding the current injection well and areas northwest of the well compose the primary reservoir for current injection operations. This reservoir appears to be bounded by normal Fault 3 to the east and possibly the absence of the Leadville formation (due to erosion) or an unmapped fault to the west, and, in model 1, partially bounded by the strike-slip fault to the south (Fig. 14). Both models indicate that the fault blocks south of the well are offset to the east, either by displacement along a strike-slip fault (model 1; Fig. 14a) or merging and bending of Faults 1 and 2 (model 2; Fig. 14b). Hence, these models suggest that the most likely location for a second injection well in the vicinity of the current well is to the south and east of the current well. In model 1, the region south of the inferred strike-slip fault has experienced relatively little induced

Downloaded from http://gji.oxfordjournals.org/ by guest on January 7, 2015

seismicity and may be largely isolated from strong pore pressure perturbations from the current well. Hence, in this model, the region south of the strike-slip fault would appear to be a good region for the further investigations needed to select a site for a potential second injection well. If the Leadville formation is absent or of poor quality west of normal Fault 1, then a second well site location should be considered in the area east of Fault 1. However, further investigations are needed to determine if this is the case.

If model 1 is correct, then mapping of the northwest-striking normal faults, as was done during early PVU geological investigations, is not sufficient for extending the subsurface geological model several kilometres away from the current PVU injection well. The strike-slip fault we infer to be present south of the well in this model was not identified by early investigations that utilized deep seismic reflection and well data. Even with modern data acquisition and processing methods, identification and precise location of strike-slip faults, which have little vertical offset, may be difficult using seismic reflection data alone, especially with little well control available. Because additional strike-slip faults with substantial horizontal offset could be present (beyond the area illuminated by earthquake hypocentres), additional methods for subsurface investigation may be needed to help identify such faults.

CONCLUSIONS

Based on spatiotemporal analysis of precise relative hypocentres and focal mechanisms of seismic events induced by PVU fluid injection, we interpret conjugate sets of pre-existing near-vertical fractures along which the induced earthquakes expand over time. One of the two conjugate fracture orientations (set *A*) is optimally oriented in the current regional stress field for shear failure. Many of the induced seismic events have focal mechanisms consistent with slip on these fractures, and many of the epicentre lineations are parallel to their strike. For the area immediately east and southeast of the injection well, fractures oriented subparallel to the regional direction of maximum compressive stress appear to be supporting shear slip, rather than behaving as high-permeability conduits or tensile cracks. The local direction of maximum horizontal stress in this area appears to be rotated approximately 30°–35° clockwise from that of the regional stress field, at least at the depth of the target injection formation. This rotation appears to have remained relatively constant throughout injection, and therefore would seem to reflect pre-existing structure or material anisotropy. However, we cannot rule out stress-induced anisotropy arising during the early stages of injection as contributing to this stress rotation.

In addition, we analyse the spatial hypocentre patterns to develop two revised subsurface fault models for the area surrounding the PVU injection well, to distances up to 8 km from the well. In addition to refining the locations, strikes and throws of subsurface normal faults interpreted previously from seismic reflection data, in one model we propose the existence of a previously unidentified strike-slip fault with approximately 1.5 km of horizontal offset. Additional investigations are required to provide further constraints on these fault models.

The enhanced understanding of the subsurface geological structure surrounding the PVU injection well may have multiple practical applications. Improved knowledge of the subsurface geology, such as the locations of impermeable faults, has implications for future injection operations and site selection for a potential second PVU injection well. Our improved knowledge of the geological structure may help constrain estimates of the maximum magnitude earthquake that may be induced. In addition, the geological information inferred from this analysis can be used as input to computer models for simulating pore pressure and stress changes due to injection, which may lead to a better understanding of the earthquake triggering mechanisms. Such models may prove useful for determining how to conduct long-term injection operations while minimizing the associated seismic hazard.

ACKNOWLEDGEMENTS

This paper summarizes studies done in support of the PVU. We thank Andy Nicholas, Tyler Artichoker, and Ed Warner for their support of PVU seismic monitoring and analysis. We are grateful to Rick Martin, Dee Overturf, Tom Bice, Jon Ake, Dan O'Connell, Ken Mahrer, Denis Bourdeau, Mark Meremonte, Zeb Maharrey, Steve Ploetz, Steve Roberts, Dave Copeland, Glenda Besana-Ostman, Mike Gilliam and Scott Cartwright for their installation and maintenance of PVSN stations and data acquisition systems. We are grateful to PVU Consultant Review Board members Thomas Davis, Jeffrey Nunn, Maurice Dusseault and Alfred Eustes III for encouraging us to pursue this analysis and for the suggestion of a sealing fault south of the injection well. We thank Daniel Levish and Ralph Klinger for discussions of the geological models. Finally, we thank the anonymous reviewers for their constructive comments which substantially improved the paper.

REFERENCES

Ake, J., Mahrer, K., O'Connell, D. & Block, L., 2005. Deep-injection and closely monitored induced seismicity at Paradox Valley, Colorado, *Bull. seism. Soc. Am.*, **95,** 664–683.

Angus, D.A., Kendall, J.M., Fisher, Q.J., Segura, J.M., Skachkov, S., Crock, A.J.L. & Dutko, M., 2010. Modelling microseismicity of a producing reservoir from coupled fluid-flow and geomechanical simulation, *Geophys. Prospect.*, **58,** 901–914.

Baisch, S. & Harjes, H.P., 2003. A model for fluid-injection-induced seismicity at the KTB, Germany, *Geophys. J. Int.*, **152,** 160–170.

Block, L., Yeck, W., King, V., Derouin, S. & Wood, C., 2012. Review of geologic investigations and injection well site selection, Paradox Valley Unit, Colorado, Bureau of Reclamation, Technical Memorandum No. 86-68330-2012-27, pp. 71.

Block, L.V., 1991. Joint hypocenter-velocity inversion of local earthquake arrival time data in two geothermal regions, *PhD thesis*, Massachusetts Institute of Technology, Cambridge, MA.

Block, L.V., Wood, C.K., Yeck, W.L. & King, V.M., 2014. The 24 January 2013 ML 4.4 earthquake near Paradox, Colorado and its relation to deep well injection, *Seismol. Res. Lett.*, **85,** 609–624.

Bremkamp, W. & Harr, C.L., 1988. Area of least resistance to fluid movement and pressure rise, Paradox Valley unit Salt Brine Injection Project, Bedrock, Colorado, Report to the Bureau of Reclamation, pp. 39.

Bremkamp, W., Harr, C.L. & Prather, O.E., 1984. Geophysical interpretation—seismic data, Paradox Valley Unit, Montrose County, Colorado, Report 3-CS-40-0146B to Bureau of Reclamation, pp. 24.

Bruno, M.S. & Winterstein, D.F., 1994. Some influences of stratigraphy and structure on reservoir orientation, *Geophysics*, **59,** 954–962.

Campbell, J.A., 1981. Summary of Paleozoic stratigraphy and history of western Colorado and eastern Utah, in *Proceedings of the New Mexico Geological Society Thirty-Second Field Conference*, pp. 81–88, eds Epis, R.C. & Callender, J.F., New Mexico Geological Society.

Cater, F.W., 1970. Geology of the Salt Anticline Region in Southwestern Colorado, U.S. Dept. of the Interior, U.S. Geological Survey Professional Paper 637, pp. 75.

Clark, S.P., 1966. *Handbook of Physical Constants*, Vol. 97, Geological Society of America.

Downloaded from http://gji.oxfordjournals.org/ by guest on January 7, 2015

Doelling, H.H., 1998. Geology of Salt Valley anticline and Arches National Park, Grand County, Utah, in *Proceedings of the Salt Deformation in the Paradox Region*, Utah Geological and Mineral Survey Bulletin 122, pp. 58, eds Doelling, H.H., Oviatt, C.G. & Huntoon, P.W., Salt Lake City, Utah.

Envirocorp Services and Technology Inc., 1995. Report of Evaluation of Injection Testing for Paradox Valley Injection Test No. 1, Report to Bureau of Reclamation, pp. 67, Durango, CO.

Fagan, D., van Wijk, K. & Rutledge, J., 2013. Clustering revisited: a spectral analysis of microseismic events, *Geophysics*, **78,** KS41–KS49.

Fossum, A.F. & Fredrich, J.T., 2002. Salt mechanics primer for near-salt and sub-salt deepwater Gulf of Mexico field developments, Sandia National Laboratories, SAND2002-2063.

Friedman, J.D., Case, J.E. & Simpson, S.L., 1994. Tectonic trends of the northern part of the Paradox Basin, southeastern Utah and southwestrn Colorado, as derived from Landsat Multispectral Scanner imaging and geophysical and geologic mapping, in *Evolution of Sedimentary Basins—Paradox Basin*, pp. C1–C30, ed. Huffman, A.C.J., U.S. Geological Survey.

Grout, M.A. & Verbeek, E.R., 1998. Tectonic and paleostress significance of the regional joint network of the Central Paradox Basin, Utah and Colorado, in *Proceedings of the Laccolith Complexes of Southeastern Utah: Tectonic Control and Time of Emplacemente Workshop Proceedings*, US Geological Survey Bulletin 2158, pp. 151–156, eds Friedman, J.D. & Huffmann, A.C., Denver, CO.

Gutierrez, F., 2004. Origin of the Salt Valleys in the Canyonlands section of the Colorado Plateau—evaporite-dissolution collapse versus tectonic subsidence, *Geomorphology*, **57,** 423–435.

Hardebeck, J.L. & Michael, A.J., 2006. Damped regional-scale stress inversions: methodology and examples for southern California and the Coalinga aftershock sequence, *J. geophys. Res.: Solid Earth*, **111,** B11310, doi:10.1029/2005JB004144.

Harr, C.L., 1988. Final geological well report, Bureau of Reclamation Injection test well no. 1, Paradox Valley, Montrose County, Colorado, Report to Bureau of Reclamation, pp. 141.

Heidbach, O., Tingay, M., Barth, A., Reinecker, J., Kurfeß, D. & Müller, B., 2008. The world stress map database release in WSM. Rel2008.

Herwanger, J.V., Mohamed, F.R., Newman, R. & Vejbaek, O., 2013. Time-lapse seismic data-calibrated geomechanical model reveals hydraulic fracture re-orientation, in *Proceedings of the SEG Houston 2013 Annual Meeting*, Society of Exploration Geophysicists, Houston, TX, pp. 4949–4953.

Hite, R.J., 1975. An unusual northeast-trending fracture zone and its relations to basement wrench faulting in northern Paradox Basin, Utah and Colorado, in *Proceedings of the 8th Field Conference*, pp. 217–223, Four Corners Geological Society Cayonlands: Durango.

Katz, L.J. & Carroll, R., 1984. Geophysical Interpretation of Seismic Data, Paradox Valley Unit, Report to Buerau of Reclamation, Utah Geophysical, Inc., pp. 31.

King, V.M., Block, L.V., Yeck, W.L., Wood, C.K. & Derouin, S.A., 2014. Geological structure of the Paradox Valley Region, Colorado, and relationship to seismicity induced by deep well injection, *J. geophys. Res.: Solid Earth*, **119,** 4955–4978.

Kluth, C.F. & DuChene, H.R., 2009. Late Pennsylvanian and early Permian structural geology and tectonic history of the Paradox Basin and Uncompahgre Uplift, Colorado and Utah, in *The Paradox Basin Revisited—New Developments in Petroleum Systems and Basin Analysis*, pp. 178–197, eds Houston, W.S., Wray, L.L. & Moreland, P.G., Rocky Mountain Association of Geologists.

Lee, S.H. & Ghassemi, A., 2010. A three-dimensional thermo-poro-mechanical finite element analysis of a wellbore on damage evolution, in *Proceedings of the 44th U.S. Rock Mechanics Symposium and 5th U.S.-Canada Rock Mechanics Symposium*, pp. 228–238, American Rock Mechanics Association, Salt Lake City, UT.

Luo, G., Nikolinakou, M.A., Flemings, P.B. & Hudec, M.R., 2012. Geomechanical modeling of stress adjacent to salt bodies: Part 1—uncoupled models, *AAPG Bull.*, **96,** 43–64.

Martinez-Garzon, P., Bohnhoff, M., Kwiatek, G. & Dresen, G., 2013. Stress tensor changes related to fluid injection at the Geysers geothermal field, *Geophys. Res. Lett.*, **40,** 2596–2601.

Martínez-Garzón, P., Kwiatek, G., Ickrath, M. & Bohnhoff, M., 2014. MSATSI: A MATLAB package for stress inversion combining solid classic methodology, a new simplified user-handling, and a visualization tool, *Seismol. Res. Lett.*, **85,** 896–904.

McKenzie, D.P., 1969. The relation between fault plane solutions for earthquakes and the directions of the principal stresses, *Bull. seism. Soc. Am.*, **59,** 591–601.

Moriya, H., Niitsuma, H. & Baria, R., 2003. Multiplet-clustering analysis reveals structural details within the seismic cloud at the Soultz geothermal field, France, *Bull. seism. Soc. Am.*, **93,** 1606–1620.

Nikolinakou, M.A., Luo, G., Hudec, M.R. & Flemings, P.B., 2012. Geomechanical modeling of stress adjacent to salt bodies: Part 2—poroelastoplasticity and coupled overpressures, *AAPG Bull.*, **96,** 65–85.

Rowe, C.A., Aster, R.C., Borchers, B. & Young, C.J., 2002. An automatic, adaptive algorithm for refining phase picks in large seismic data sets, *Bull. seism. Soc. Am.*, **92,** 1660–1674.

Sayers, C.M., 1998. Misalignment of the orientation of fractures and the principal axes for P and S waves in rocks containing multiple non-orthogonal fracture sets, *Geophys. J. Int.*, **133,** 459–466.

Scholz, C.H., 2002. *The Mechanics of Earthquakes and Faulting*, Cambridge Univ. Press.

Singhal, B. & Gupta, R., 2010. Fractures and discontinuities, in *Applied Hydrogeology of Fractured Rocks*, 2nd edn, pp. 13–33, Springer.

Snieder, R. & Vrijlandt, M., 2005. Constraining the source separation with coda wave interferometry: theory and application to earthquake doublets in the Hayward fault, California, *J. geophys. Res.*, **110,** B04301, doi:10.1029/2004JB003317.

Snoke, J.A., 2009. *FOCMEC: FOCal MEChanism determinations*, Virginia Tech, pp. 22.

Song, F., Kuleli, H.S., Toksoz, M.N., Ay, E. & Zhang, H., 2010. An improved method for hydrofracture-induced microseismic event detection and phase picking, *Geophysics*, **75,** A47–A52.

Steenland, N.C., 1962. Gravity and aeromagnetic exploration in the Paradox Basin, *Geophysics*, **28,** 73–89.

Stevenson, G.M. & Baars, D.L., 1986. The paradox: a pull-apart basin of Pennsylvanian age, in *Paleotectonics and Sedimentation in the Rocky Mountain Region, United States*, pp. 513–539, ed. Peterson, J.A., Utah Geological Survey.

Thomas, W.A., 2007. Pennsylvanian sinistral faults along the southwest boundary of the uncompahgre uplift, Ancestral Rocky Mountains, Colorado, *Geosphere*, **3,** 119–132.

Trudgill, B.D., 2011. Evolution of salt structures in the northern Paradox Basin: controls on evaporite deposition, salt wall growth and supra-salt stratigraphic architecture, *Basin Res.*, **23,** 208–238.

Verdon, J.P., Kendall, J.M., White, D.J. & Angus, D.A., 2011. Linking microseismic event observations with geomechanical models to minimise the risk of storing CO_2 in geological formations, *Earth planet. Sci. Lett.*, **305,** 143–152.

Winterstein, D. & Meadows, M., 1991. Shear-wave polarizations and subsurface stress directions at Lost Hills field, *Geophysics*, **56,** 1331–1348.

Wuestefeld, A., Kendall, J.M., Verdon, J.P. & van As, A., 2011. *In situ* monitoring of rock fracturing using shear wave splitting analysis: an example from a mining setting, *Geophys. J. Int.*, **187,** 848–860.

Downloaded from http://gji.oxfordjournals.org/ by guest on January 7, 2015